Title

Long-Distance Trail Running Induces Inflammatory-Associated Protein, Lipid, and Purine Oxidation in Red Blood Cells

Authors

Travis Nemkov,[1*] Emeric Stauffer,[2,3,4] Francesca Cendali,[1] Daniel Stephenson, [1] Elie Nader,[2,3] Mélanie Robert,[2,3,5] Sarah Skinner,[6] Monika Dzieciatkowska,[1] Kirk C. Hansen,[1] Paul Robach,[7] Guillaume Millet,[8] Philippe Connes,[2,3] Angelo D'Alessandro,[1*]

Affiliations

1) Department of Biochemistry and Molecular Genetics, University of Colorado Denver – Anschutz Medical Campus, Aurora, CO, USA;
2) Laboratoire Interuniversitaire de Biologie de la Motricité (LIBM) EA7424, Team "Vascular Biology and Red Blood Cell", Université Claude Bernard Lyon 1, Université de Lyon, Lyon, France;
3) Laboratoire d'Excellence du Globule Rouge (Labex GR‐Ex), PRES Sorbonne, Paris, France;
4) Centre de Médecine du Sommeil et des Maladies Respiratoires, Hôpital Croix Rousse, Hospices Civils de Lyon, Lyon, France;
5) Erytech Pharma, Lyon, France;
6) Unité de Recherche Clinique et Epidémiologie (URCE), Centre Hospitalier Universitaire de Montpellier, Montpellier, France
7) National School for Mountain Sports, Site of the National School for Skiing and Mountaineering, Chamonix, France
8) Laboratoire Interuniversitaire de Biologie de la Motricité (LIBM) EA7424, Team "Vascular Biology and Red Blood Cell", Université Jean-Monnet, Saint-Etienne, France

***Corresponding authors:**

Travis Nemkov, PhD
Department of Biochemistry and Molecular Genetics
University of Colorado Anschutz Medical Campus
12801 East 17th Ave., Aurora, CO 80045
Phone # 303-724-3253
E-mail: travis.nemkov@cuanschutz.edu

Angelo D'Alessandro, PhD
Department of Biochemistry and Molecular Genetics
University of Colorado Anschutz Medical Campus
12801 East 17th Ave., Aurora, CO 80045
Phone # 303-724-9121
E-mail: angelo.dalessandro@cuanschutz.edu

Abstract

Ultra-endurance exercise places extreme physiological demands on oxygen transport, yet its impact on red blood cells (RBCs) remains underexplored. We conducted a multi-omics analysis of plasma and RBCs from endurance athletes before and after a 40-km trail race (MCC) and a 171-km ultramarathon (UTMB®). Ultra-running led to oxidative stress, metabolic shifts, and inflammation-driven RBC damage, including increased acylcarnitines, kynurenine accumulation, oxidative lipid and protein modifications, reduced RBC deformability, enhanced microparticle release, and decreased hematocrit – hallmarks of accelerated RBC aging and clearance. Post-race interleukin-6 strongly correlated with kynurenine elevation, mirroring inflammatory responses in severe infections. These findings challenge the assumption that RBC damage in endurance exercise is primarily mechanical, revealing systemic inflammation and metabolic remodeling as key drivers. This study underscores RBCs as both mediators and casualties of extreme exercise stress, with implications for optimizing athlete recovery, endurance training, and understanding inflammation-linked RBC dysfunction in clinical settings.

Teaser

Marathon running imparts molecular damage to red blood cells, the effects of which are exacerbated by increased distances of ultramarathons.

MAIN TEXT

Introduction

Endurance exercise places significant demands on the oxygen transport system, and red blood cells (RBCs) are at the forefront of meeting these challenges. In addition to delivering oxygen and removing carbon dioxide, RBCs contribute to pH buffering and release signaling molecules—such as ATP and nitric oxide—that facilitate vasodilation and enhance muscle perfusion (*1, 2*). While moderate exercise is associated with improved cardiovascular function and metabolic health, prolonged endurance events like marathons and ultramarathons impose additional mechanical, metabolic, and oxidative stresses. These stressors can result in acute cellular damage particularly in RBCs, where the capacity for repair is limited owing to the lack of nuclei and organelles that results in the incapacity to replace damaged protein and lipid components through *de novo* synthesis (*3*).

Historically, investigations into exercise physiology have largely focused on skeletal muscle (*4*), serum (*5*), and plasma (*6*) biomarkers to gauge the systemic impact of prolonged running. However, emerging evidence suggests that the RBC compartment provides critical insights into the cellular adaptations and injury responses elicited by extreme exercise (*7, 8*). Yet, classic concepts like footstrike hemolysis – also known as march hemoglobinuria, first described by Fleischer in 1881 (*9*) – have been recently challenged in comprehensive reviews (*10*), which indicates an incomplete understanding of the role of RBC biology in exercise tolerance and performance. Recent advances in multiomics technologies have opened new avenues for comprehensively mapping the molecular responses to strenuous exercise. Simultaneously interrogation of the metabolome, lipidome, proteome, and metallome, now enables holistic understanding of how tissues and circulating cells respond to exercise-induced stress. Studies have highlighted that transient cytokine release (e.g., interleukin-6) during endurance exercise triggers metabolic remodeling and tissue repair (*11, 12*), in addition to oxidative modifications in RBC, shifts in membrane lipid composition, and ultimately compromised RBC deformability (*7*).

Despite these advances, the specific molecular responses of RBCs to prolonged endurance exercise remain insufficiently characterized. This knowledge gap is particularly relevant in the context of long-distance trail running, where additional challenges such as variable terrain, altitude, and prolonged mechanical stress further compound the injury and repair processes in RBCs. Indeed, long distance running results in appreciable damage to RBC including decreased deformability and increased markers

of senescence (*13, 14*) in the face of increased inflammation (*15*). Previous omics-based studies have predominantly focused on plasma responses to acute exercise or short-duration laboratory tests (*16*), ultramarathon treadmill simulations (*17*), or *in situ* (*18, 19*), which cannot recapitulate the unique stressors encountered during ultra-endurance events in the outdoors [reviewed in (*20*)]. Moreover, while plasma-based analyses provide valuable systemic information, they do not capture the direct impact on RBCs—cells that lack nuclei and organelles and are thus uniquely dependent on metabolic pathways to cope with oxidative damage.

In light of these considerations, our study was designed to integrate multi-omics approaches to delineate the impact of long-distance trail running on both plasma and RBC molecular signatures. By comparing pre- and post-race samples from athletes competing in the World Class Martigny–Combes à Chamonix race (MCC, 40 km, elevation gain: 2300 m) and Ultra-Trail du Mont Blanc race (UTMB©, 171 km, elevation gain: 10,000 m), we aimed to elucidate the distinct metabolic, inflammatory, and oxidative modifications that occur with increasing exercise duration. We hypothesized that while both marathon and ultramarathon events trigger systemic inflammatory responses and metabolic remodeling, the extent of cellular damage—particularly within the RBC compartment—would be more pronounced in ultramarathon running.

Results

Molecular responses to ultra-running in plasma and RBCs

To characterize molecular changes in both plasma and RBCs as a function of running distance, samples were isolated from 23 runners, divided as follows: (i) 11 runners (5 female, 6 male, age 35.7 ± 8.6 years, BMI 21.75 ± 2.81 kg/m^2) before (Pre) and immediately after (Post) the MCC; or (ii) 12 runners (4 female, 8 male, age 38 ± 6.4 years, BMI 21.56 ± 1.53 kg/m^2) before (Pre) and immediately after (Post) the (UTMB). In addition to assessing hematological and rheological parameters (*14*), mass spectrometry-based metabolomics, lipidomics, trace element analysis (i.e. metallomics), and proteomics profiles were determined (**Figure 1A**). After curation, these analyses provided quantitative data in plasma or RBCs on 440 or 1105 proteins, 659 or 647 lipids, 197 or 271 metabolites, and 8 or 6 metals, respectively (**Figure 1B, Supplementary Tables 1 and 2**). Using the entire dataset, Partial Least Squares-Discriminant Analysis (PLS-DA) separated Pre from Post plasma samples along Component 1, which explained 11.1% or 17.5% of the data variance in the MCC or UTMB, respectively (**Figure 1C-D**). While MCC plasma was largely characterized by increases in acyl-carnitines (AC) and fatty acids (FA), UTMB plasma showed decreased levels of lysophospholipids (LP) and increases in the purine catabolite, hypoxanthine, muscle creatine kinase (KCRM), and acute phase response proteins CRP, SAA1, SAA2 (**Figure 1C-D**). Similarly, RBCs after the MCC had increased AC (including hydroxylated), FA, and decreased coenzyme A precursor pantothenate, while RBCs after the UTMB had elevated levels of (hydroxy)AC, the oxylipin 13(S)-HODE, and tryptophan catabolite, kynurenine (**Figure 1E-F**). There was no difference in VO_2max between the two groups of runners, and although MCC runners tended to run at a faster pace, there was no significant correlation between run speed and VO_2max (**Figure 1G**). However, a linear mixed model of run speed (adjusted for age, sex, and BMI) and molecular fold changes (Post/Pre) showed significant associations with 51 plasma molecules that largely included lipids such as phosphatidylcholines (PC), acylcarnitines (AC), cholesteryl esters (ChE), ceramides (Cer), sphingomyelins (SM), diacylglycerides (DG), and triacylglycerides (TG), without or with ether (O-) linkages (**Figure 1H**). This model also highlighted tryptophan metabolism (kynurenine, kynurenate, indolepyruvate), and transferrin receptor (TFR1), which mediates cellular iron uptake. Meanwhile, only the RBC level of adenosine diphosphate (ADP) was significantly associated with run speed (**Figure 1I**).

Inflammatory markers increase in the plasma after ultra-running

In consideration that molecular signatures in the plasma are associated more strongly with run time, we next identified signatures with respect to individual molecular class (i.e. proteins, metabolites, lipids). Reflecting the strong lipidomic signature associated with both speed and distance, MCC and UTMB plasma had significantly decreased diacylglycerides (DG), while UTMB alone also had significant decreases in lysophosphatidylcholines (LPC), lysophosphatidylethanolamines (LPE), and cardiolipins (CL), alongside increased acylcarnitines (**Figure 2A**). Active lipid metabolic pathways during both MCC and UTMB were mapped using Bioinformatics Methodology For Pathway Analysis (BioPAN) (*21*) and revealed distinct lipid remodeling patterns between the two races (**Figure 2B, Supplementary Table 3**). In UTMB, the lysophosphatidylethanolamine (LPE) → phosphatidylethanolamine (PE) → phosphatidylserine (PS) axis was significantly enriched, suggesting an increased demand for PE and PS. In contrast, MCC exhibited a stronger conversion of PE to phosphatidylcholine (PC) likely driven by phosphatidylethanolamine N-methyltransferase (PEMT) activity, indicating a preference for PC biosynthesis over PS production. Additionally, UTMB showed a pronounced increase in ether lipid remodeling (O-LPC → O-PC), while MCC displayed a broader remodeling of glycerophospholipids, particularly in PC and LPS pathways. These differences highlight distinct metabolic adaptations between the two conditions, reflecting variations in membrane composition, lipid signaling, and phospholipid homeostasis.

Changes in the plasma proteome contained fewer significant differences, although the number of significantly increased proteins after the race was higher in the UTMB cohort (**Supplementary Figure 1**). When comparing fold changes at completion of each race to baseline values, and consistent with the race-specific lipidomics signatures noted above, post-race elevation of the fatty acid transporter and immunomodulator CD36 (*22*) was observed particularly in MCC runners (**Figure 2C**). On the other hand, UTMB runners presented with larger increases in creatine kinase muscle-type (KCRM), which is indicative of ongoing skeletal muscle damage (*23*) (**Figure 2C**). In addition, compared to MCC, UTMB runners had elevations in numerous proteins involved in the acute phase response including Serum Amyloid A1 and A2 (SAA1 and SAA2) and LPS-binding protein (LBP), which plays a critical role in the innate immune response to bacterial infections. In support of these proteomics data, the circulating levels of multiple cytokines (*15*) including IL-6 were significantly higher in runners after both races, with a trend towards higher elevations after the UTMB (**Figure 2D**). As such, a Debiased Sparse Partial Correlation (DSPC) network (*24*) of IL-6 revealed several associations with total white blood cell counts, inflammatory proteins (CRP, SAA1, SAA2, SAA4, LBP, A2GL, A1AG1), cytosolic proteins (TKT, MDHC, LDHB), carboxylic acids (citrate, succinate, fumarate, malate), purine catabolites (hypoxanthine, urate), acylcarnitines, and fatty acids (**Figure 2E, Supplementary Figure 2**). Lipid pathways that correlated with IL-6 levels centered largely upon DG and LPC conversion into PC (**Figure 2F**). Plasma metabolites that correlated with IL-6 levels were significantly involved in linoleic acid metabolism, though there was substantial representation from mitochondrial pathways including the Citric Acid Cycle, Urea Cycle, branched chain amino acid oxidation, and metabolism of many amino acids (**Figure 2G**). Gene ontology (GO) analysis of proteins that were positively correlated with IL-6 confirmed acute inflammatory response, while downregulated proteins were involved in cholesterol trafficking (lipoprotein particle assembly), complement activation, coagulation, regulation of body fluid levels, and wound healing (**Figure 2H**). Interestingly, negative correlated proteins F13B and MASP1 have also been associated with COVID-19 pathology (**Figure 2I**). Kynurenine was an additional molecular correlate with IL-6 (**Figure 2E, Supplementary Figure 2**), also consistent with this reportedly strong positive association in COVID-19 disease severity.(*25-27*) While kynurenine levels significantly correlated between the plasma and RBCs fractions in this study (**Figure 2J**), RBC kynurenine levels in particular were the strongest molecular correlate with IL-6 across the entire dataset (**Figure 2K, Supplementary Figures 3-4**), consistent with the hypothesis that uptake via SLC7A5 (LAT1) favors a role for RBCs as a circulating reservoir of metabolic markers of systemic inflammation.(*28*)

RBCs accumulate damage markers specifically during ultra-running

In light of the strong link between RBC molecular signatures and inflammation, and the recently reported association between elevated RBC kynurenine levels and increased susceptibility to hemolysis (*28*), we next turned to in depth analysis of the RBC fraction. Multiple changes to RBC characteristics were distinctly observed after running a marathon or ultra-marathon distance (**Figure 3A**). Namely, mean cell volume (MCV) decreased after both races in line with increases in immature reticulocytes. While elevations in PS-exposing RBCs (a marker of eryptosis (*29-31*)) were observed after the MCC, PS-exposing RBCs were unchanged after the UTMB. However, UTMB runners showed an increase in circulating RBC-derived microparticles in addition to an appreciable reduction in hematocrit. To determine molecular changes to RBCs as they pertain to running distance, PLS-DA using fold change data (Delta = Post/Pre) was able to distinguish RBCs from each race (**Figure 3B**). The molecules that most strongly influenced this clustering pattern included urate, creatinine, medium chain acyl-carnitines, and LPCs – higher after MCC – or long chain acylcarnitines, carboxylic acids (fumarate, methylmalonate), carnitine, and copper – higher after UTMB (**Figure 3C**).

RBCs activate Lands Cycle for membrane lipid repair during marathon and ultra-marathon running

Changes in the abundance of multiple lipid classes as a whole occurred during both races (**Figure 4A**). Notably, acylcarnitines were significantly elevated after the UTMB in conjunction with decreased LPC. In RBCs, these lipid classes are central to the Lands Cycle, a process by which RBCs replace oxidatively damaged membrane lipid acyl chains using a pool of acyl-CoA molecules that are interconverted with acylcarnitines based on demand for lipid repair (**Figure 4B**). Interrogation of specific free fatty acids (**Figure 4C**) and acylcarnitines (**Figure 4D**) highlighted increased levels after each race. In line with an activated Lands cycle, the ratio of lysophospholipids-to-phospholipids (specifically LPC/PC and LPE/PE) were lower after each race (**Figure 4E**). The extent of both fatty acid and medium chain acylcarnitine accumulation was higher in RBCs after the MCC, while post-UTMB RBCs maintained comparable levels of long chain acylcarnitines including the most abundant AC(18:1). RBCs rely on pantothenate to synthesize CoA, which significantly decreased after both races. On the other hand, carnitine was significantly elevated after the UTMB (**Figure 4F**), suggesting decreased utilization for synthesis of acylcarnitines in these RBCs.

Lipid network analysis using BioPAN revealed distinct lipid remodeling patterns in RBCs between MCC and UTMB (**Figure 4G and 4H, Supplementary Table 4**). In MCC, RBCs exhibited a stronger PE → PC remodeling pathway mediated by PEMT. Additionally, MCC showed significant ether lipid remodeling (O-LPC → O-PC), driven by Lysophosphatidylcholine Acyltransferase 3 (LPCAT3), which is linked to Lands cycle activation, ferroptosis and extravascular hemolysis (*32*). This pattern suggests increased oxidative stress, as ether lipids play a crucial role in protecting RBCs membranes from lipid peroxidation (*33*). In contrast, UTMB RBCs exhibited a stronger shift toward phosphatidylserine (PS), with significant activity in PC → PS ($Z = 2.267$) and PE → PS ($Z = 1.779$) conversions that are mediated by PTDSS1 and PTDSS2 (Phosphatidylserine Synthases 1 & 2). These reactions, along with the LPE → PE → PS → LPS pathway, indicate a preference for redistributing phospholipids within the membrane. However, there was no corresponding increase in PS externalization (**Figure 3A**), suggesting that the population of RBCs in circulation after the UTMB maintained membrane asymmetry as a function of increased ATP-dependent flippase activity.

Distinct differences between MCC and UTMB in fatty acid homeostasis was observed as well (**Figure 4G** and **4H**). RBCs from both races displayed increased fatty acid desaturation activity – conversion of FA(16:0) → FA(16:1) and FA(18:0) → FA(18:1) via FADS5. However, MCC RBCs demonstrated increased FA(18:2) → FA(18:3) conversion ($Z = 0.899$), while this conversion was notably larger ($Z = 2.052$) in UTMB RBCs. As this step is carried out by Fatty Acid Desaturase 2 (FADS2), which

is present in RBCs and active in maintaining NAD/NADH ratios under oxidant stress (*34*), differences between RBCs during MCC and UTMB suggesting altered networks to maintain redox homeostasis in the face of ongoing endurance running.

Additionally, eicosanoid and oxidized lipid species showed differential regulation between MCC and UTMB (**Figure 4I**). While HETEs (hydroxyeicosatetraenoic acids) remained unchanged (**Supplementary Table 2**), significant ($p < 0.05$) increases were observed in MCC of several hydroxy derivatives (including 9(S)- and 13(S)-HODE), hydroperoxy derivatives (including 9(S)-HpOTrE, 12(S)-HpETE, 15(S)-HpEDE, 9(S)- and 13(S)-HpODE, and 15(S)-HpEPE), which are formed by lipoxygenase-mediated or non-enzymatic auto-oxidation of polyunsaturated fatty acids. Moreover, increases in downstream metabolites, such as oxo forms (including 9(S)- and 13(S)-oxoODE) and dihydroxy forms (including 9(10)- and 12(13)-diHOME), indicate significantly increased lipid peroxidation and oxidative stress in MCC RBC, while these molecules approach significance ($p < 0.08$) in UTMB RBC.

Prolonged running activates purine salvage and alternative carboxylate metabolism

Because they are devoid of mitochondria, RBCs depend solely on glycolysis for ATP production. RBCs after the MCC were not different aside from significantly accumulated lactate (**Supplementary Figure 5**). However, the UTMB elicited significant accumulations in multiple glycolytic intermediates aside from pyruvate and lactate that trended higher, but did not reach significance. Increased phosphoenolpyruvate/pyruvate ratios in UTMB, but not MCC, is consistent with inhibition of redox sensitive pyruvate kinase (PK). However, it remains to be assessed whether pharmacological PK activation could be beneficial in the context ultra-marathon, in that PK activation would come at the cost of 2,3-BPG depletion (*35*) thus counteracting the beneficial effects this molecule has towards hemoglobin allostery by favoring O2 off-loading. Similarly, RBCs after the UTMB had lower oxidative phase Pentose Phosphate Pathway (PPP) intermediates and higher end-products (ribose phosphate and pentose phosphate isomers), including downstream non-oxidative phase sedoheptulose phosphate, which is suggestive of an active flux through this pathway.

The PPP is used to generate NADPH for oxidative stress management, which impacts purine levels that are maintained through the purine salvage pathway (*36*). RBCs after the MCC had higher inosine and urate, indicative of purine catabolism (**Figure 5A**). In contrast, RBCs after the UTMB had higher IMP and hypoxanthine, which is derived from oxidant stress activation of AMPD3 to trigger purine breakdown and deamination (*37*). Subsequent decreases in xanthine and allantoate are further indicative of purine salvage rather than catabolism. This pathway relies upon aspartate, which is used by adenylosuccinate synthase (ADSS) to convert IMP back into AMP. The metabolic signature of carboxylic acids in UTMB RBCs demonstrates increased utilization of aspartate in this process (**Figure 5B**). In addition, elevated levels of malate suggest activation of the GOT1/MDH axis to recycle NAD^+, in similar fashion to previous studies of RBCs during acclimatization to high altitude or hypoxic storage in the blood bank (*38*). Similarly, pyruvate/lactate ratios were higher both at baseline and after the race in UTMB compared to MCC (**Figure 5C**), suggestive of the activation of methemoglobin (MetHb) reductase. Indeed, as LDH and MetHb reductase compete for NADH as a substrate, elevation in pyruvate/lactate ratios reflect oxidant metabolic defects in RBCs, such as in the case of G6PD deficiency (*39, 40*).

The RBC proteome accumulates oxidative damage during marathon and ultra-marathon running

After establishing the impact of both MCC and UTMB – especially the latter – in triggering oxidant stress to RBCs, we then sought to determine the impact of running distance on protein homeostasis, given the incapacity of mature RBCs to replace oxidatively damaged proteins via *de novo* protein synthesis and the concurrent reliance of aging RBCs on proteasomal machinery to remove damaged proteins (*41*). To this end, RBC proteomics data were mined for redox-related post-translation modifications (PTM)

including methionine oxidation, asparagine deamidation, and glutamate/aspartate methylation, all of which are marks of protein damage and repair in RBCs (*42*). Unsupervised principal component analysis (PCA) using peptide level data (including PTMs) was capable of distinguishing Pre from Post samples in both races across component 1, which described 44.3% of the data variance (**Figure 6A, Supplementary Table 5**). Of the multiple PTMs detected across the proteome, only methionine oxidation was significantly elevated after both the MCC and UTMB (**Figure 6B**). Correlating total PTM levels with hematological and blood rheological parameters including plasma viscosity, RBC deformability, microparticle generation, and cell volume revealed that methionine oxidation had the largest number of positive correlates and carbamidomethylated cysteine – a marker of reduced thiol content – had the largest number of negative correlations (**Figure 6C**). Total carbamidomethyl cysteine content was negatively ($R < 0.75$) associated with runner body fat percentage and IL-6 levels (**Figure 6C**). In parallel, specific positive correlates with methionine oxidation (Pearson $R > 0.75$) consisted of blood rheological parameters including blood viscosity and RBC deformability (EI – elongation index) as well as runner age, while the top negative correlate was the reduced (GSH) to oxidized (GSSG) glutathione ratio (**Figure 6C**). Furthermore, the top 100 peptides by ANOVA exclusively contained methionine oxidation (**Figure 6D**). RBCs after the UTMB, however, contained a higher degree of methionine oxidation when looking at modified peptide as a function of total peptide signal (**Figure 6E**), thereby indicating an increased degree of proteome oxidation in these samples. KEGG pathway analysis of proteins with statistically significant (ANOVA FDR < 0.05) increases in methionine oxidation revealed a substantial impact to components within the proteasome, Pentose Phosphate Pathway, and redox proteostasis including cysteine, methionine, and glutathione metabolism (**Figure 6F, Supplemental Figure 6**). Multiple neurodegenerative pathways were also enriched including Spinocerebellar ataxia, Parkinsons disease, Huntington disease, Alzheimer disease, and Amyotrophic lateral sclerosis. These pathways largely share proteasome, redox, and cytoskeletal proteins (**Supplementary Figure 7B**). Collectively, these analyses indicate an enrichment in four main categories of proteins, rather than random oxidation events:

i) Antioxidant enzymes: PRDX6, PCMT1 – which participates in isoaspartyl damage repair (*42*) – a modification that was elevated in MCC RBCs after the race – (**Figure 6B)**; GCLM/GSTO - linked to GSH synthesis and utilization; HPRT1 - linked to purine salvage; LTA4H - linked to eicosanoid metabolism;

ii) Metabolic enzymes: BPGM, PGD, BLVRB, ACLY – explaining in part the observed changes in 2,3-BPG levels, PPP and CoA homeostasis and citrate levels – **Supplementary Figure 5**);

iii) Ubiquitination systems and proteasome components: UBA1, UBE2V2, PSMC3; in the context of the ubiquitin system, the active site cystine within E1 and E2 enzymes forms a thioester bond with ubiquitin, facilitating its activation and transfer for ubiquitination (*43*); however, specific searches for post-translational markers of ubiquitination (K-GG modification) showed no significant changes between baseline and completion in either of the two races – (**Figure 6B)**;

iv) Structural proteins: SPTA1, SPTB, ANK1, SLC4A1, DMTN, STOM, ADD – consistent with elevated microparticle release (**Figure 3A**) and suggestive of impaired RBC deformability.

RBC deformability correlates with protein homeostasis and copper

Given the significant accumulations of lipid and protein oxidation, inflammatory response (specifically IL-6 and kynurenine), and decreased hematocrit after the UTMB, we next focused on blood rheological parameters. Hematological and blood rheological parameters were assessed before and after each race (*14*) including blood viscosity and RBC deformability (**Supplementary Figure 8**). While blood viscosity showed variable changes (increasing at 11.5 cP/s after MCC and decreasing at 225 cP/s after

UTMB), RBC deformability was markedly decreased at higher shear stresses specifically after UTMB. Integration of the area under the shear stress vs EI curve for each participant enabled calculation of a single RBC deformability value, which significantly decreased after the UTMB (**Figure 7A**). This approach also allowed for correlation of all multi-omics measurements with composite RBC deformability and revealed significant positive correlations with metabolites involved in nitrogen metabolism (lysine, proline, xanthine, ornithine), while glycolytic intermediates (2/3-phosphoglycerate, 2,3-BPG) and hydroxyacyl-carnitines including AC(14:0-OH), AC(14:1-OH) and AC(16:1-OH) were significant negative correlates (**Figure 7B**). GO enrichment of significantly correlated proteins highlighted proteasome assembly as the most enriched term (**Figure 7C, top**). Despite significantly correlating with RBC deformability, PSMA2, PSMD7, and multiple other proteasome subunits did not demonstrably change in abundance after either MCC or UTMB (**Figure 7D**). However, when factoring in PTM status on proteasome subunits, increased methionine oxidation (node size is proportional to average fold change for both races) inversely correlated with RBC deformability (**Figure 7E**). Therefore, these results implicate accumulating proteasome oxidation that could impair its activity to remove damaged proteins with decreasing RBC deformability. Additional correlations with RBC deformability were observed with metals (**Figure 7F**). Potassium, magnesium, and iron had weak positive correlations with EI at lower shear stress, though these correlations were lost (or inverted in the case of iron) at shear stresses greater than 10 Pa. Most notably, copper levels were inversely correlated with RBC deformability at all shear stresses. The concentration of copper, calcium, potassium, iron, magnesium, and sodium were elevated in RBCs specifically after the UTMB (**Figure 6G**).

Static abundant plasma analytes and increasing free bilirubin indicate increased extravascular hemolysis during ultra-running

Plasma proteomics data was mined for markers of hemolysis or blood volume increase to further interrogate the decreases in hematocrit observed specifically after the UTMB (**Figure 3A**). Despite static levels of cell free hemoglobin, intravascular hemolysis may have occurred somewhat in light of decreased haptoglobin (HP) levels (**Figure 8A**), the effects of which have been documented in distance runners (*10*). While decreased hematocrit could have also been the result of plasma volume expansion (i.e. sports anemia), the most abundant plasma proteins in the proteomics dataset including albumin and apolipoprotein A1 (ApoA-I) were unchanged in either race **(Figure 8A**). The absence of hemodilution as a cause for decreased hematocrit was further supported by unchanged levels of sodium, iron, and calcium in the plasma (**Figure 8B**). To identify molecules that associate with hematocrit, a linear mixed model was prepared that corrected for age, sex, and BMI (**Figure 8C**). The top associated feature with hematocrit was the ketone body acetoacetate. In addition, both plasma bilirubin and hypoxanthine emerged as associated features after correction. Plasma bilirubin is a marker of extravascular hemolysis (*44, 45*), and was a significant inverse correlate with hematocrit along with plasma hypoxanthine (**Figure 8D**). Hypoxanthine also increased in plasma after the UTMB (**Figure 8D**), mirroring RBC alterations (**Figure 5A**). In addition, RBC creatinine, a marker of RBC circulatory age (*46, 47*), was elevated in RBCs after both races, though to a significantly higher extent after the MCC (**Figure 8E**).

Discussion

Here we describe the impact of marathon and ultramarathon running on multi-omic (metabolomic, lipidomic, proteomic, and metallomic) profiles in plasma and RBC compartments, and how these profiles correspond to alterations in hemorheological parameters. Our findings detail the effects of ultra-running on a cascade of molecular events that extend beyond mechanical trauma, implicating systemic inflammation, oxidative stress, and metabolic remodeling as key drivers of RBC aging and dysfunction. Signatures implicate a mounting immune response that begins during a 40 km run (MCC) and accumulates during a 171 km ultramarathon (UTMB). This inflammation manifests across multiple measurement

modalities, from an increase in total white blood cell count, to elicitation of a cytokine response involving IL-6, to stimulation of the acute phase response, to production of proinflammatory metabolites such as kynurenine. These molecular signatures correspond with an initial increase after the MCC in externalized phosphatidylserine (PS) on the RBC membrane, which is a marker for RBC clearance from circulation (*48*). While elevations of external PS were not apparent in circulating RBCs after the longer UTMB race, these cells were less deformable, accompanied by decreased cell volume, higher oxidation of structural proteins, increased generation of microparticles and release of immature reticulocytes. Perhaps the most observable difference between the MCC and UTMB was decreased hematocrit during the latter race. Decreased hematocrit has been attributed specifically to increased plasma volume, termed sports anemia (*49*), though this volumetric change would have a similar effect on other abundant plasma analytes such as albumin and sodium. The fact that these corresponding effects were not observed indicates that increased plasma was not responsible for decreasing hematocrit. Rather, these results are consistent with a model positing acceleration of damage to RBC during running that results in increased splenic sequestration and extravascular hemolysis of less deformable, more damaged RBCs, in keeping with similar findings in the context of transfusion of RBCs after prolonged storage (*41*). Consistent with this hypothesis, plasma levels of bilirubin increased in accordance with decreased hematocrit, and while cell free hemoglobin remained unchanged, haptoglobin was decreased. As RBCs cross a threshold of accumulated oxidative and mechanical damage, they are selected for removal from circulation in the liver or spleen via macrophage phagocytosis (*50*). During periods of excess RBCs removal, bilirubin is released back into circulation rather than removal through the biliary duct and intestine (*44*). Therefore, these results illustrate how extended endurance running exercise results in an accelerated aging process within the RBC population, thereby leading to enhanced removal of damaged cells from circulation.

Running-induced RBC damage can stem from increased shear stress in the foot leading to mechanical trauma (*51*). Several non-mechanical injuries to RBC during exercise have also been documented that impair RBC membrane structure and deformability while promoting fragility. These mechanisms include alteration of the membrane lipidome (*7, 52*), cytoskeleton (*53, 54*), and depletion of antioxidant systems (*55*), which occur in conjunction with increased osmotic fragility due, in part, to prolonged exposure to lactate acidosis and subsequent dehydration at higher exercise intensities (*56-60*). Indeed, RBCs here decreased in volume and deformability, and while glutathione did not appear to be depleted, protein and lipid oxidation increased substantially.

We observed multiple impacts of running on the RBCs membrane lipidome. RBCs repair membrane lipid damage using the Lands Cycle, which relies on the generation of acyl-CoA substrates to replace damaged acyl chains (*61*). This process is buffered by acylcarnitines, which serve as an ATP-independent source of acyl chains (*62-64*). Therefore, carnitine availability can bolster this process and improve RBC function under extreme oxidative stress environments of blood storage (*65*). In this study, however, we observed carnitine accumulation specifically after UTMB, which might suggest that RBCs are utilizing the acyl-CoA pool at an accelerated rate and have less need for storing acyl chains in the acylcarnitine pool. Consistent depletions in both races of the CoA precursor pantothenate (Vitamin B5), which is metabolized by RBCs (*66, 67*), suggests alternative strategies to maintain the Lands Cycle during exercise provided that intestinal absorption is optimized (*68, 69*).

Double bonds in acyl chains are susceptible to hydroxylation via alpha-oxidation to generate hydroxyacylcarnitines. Inverse correlations between hydroxyacylcarnitines and RBC deformability seen here were also observed in cyclists (*7*), who do not experience similar mechanical stress in the foot, thereby indicating alternative sources of oxidative lipid stress. Notably, these molecules increase in RBC as a function of cardiorespiratory workload in a controlled cardiopulmonary exercise test (CPET) in healthy subjects (*70*). Acylcarnitine hydroxylation may occur in conjunction with increased desaturation of fatty acids, which are subsequently susceptible to lipid peroxidation (*71*). Indeed, fatty acid desaturase activity is upregulated in part to recycle NAD^+ (*72*). While the role of this pathway has been established

421 in *ex vivo* RBCs storage (*34*), future work should look at the role this pathway plays in response to exercise
422 *in vivo*.
423 The extent of oxidation on proteasome subunits inversely correlated with RBC elongation index,
424 suggesting that the loss of the RBC ability to degrade damaged proteins may be linked to loss of
425 deformability. In addition, the levels of copper were consistently inverse correlated with elongation index
426 at all shear stresses. Copper accumulation is known to occur as part of the acute phase response (*73*) and
427 can directly decrease RBC deformability (*74*) through interaction with and subsequent oxidation of
428 membrane phospholipids (*75*). Future work should focus on understanding the source of this copper (i.e.
429 extracellular versus loss of conjugation to copper-containing proteins such as superoxide dismutase, for
430 example), its direct role in RBC function, and how exercise or other stressors influence concentration
431 dynamics.
432 These results, however, do highlight the importance of oxidative stress management in circulation
433 prior to RBC removal by the reticuloendothelial system. One process by which RBCs are selected for
434 removal involves their ability to traverse the interendothelial slits within the spleen. With sub-1.5 μm
435 diameters, this transit is thus invariably dependent on the RBCs ability to deform (*76*). Moreover, passing
436 through gradients of varying tonicity in both the spleen and kidney requires that the RBCs can maintain
437 resilience to osmotic stress. Interestingly, RBCs that possess high levels of kynurenine are also
438 increasingly fragile to changes in osmotic gradients (*28*). Because kynurenine is not synthesized by RBCs,
439 its abundance is therefore a reflection of the circulating environment. Individuals who donate RBC units
440 with higher levels of kynurenine tend to be of older age or higher BMI, and the plasma proteome within
441 these units is characterized by a sterile inflammatory environment (*28*). This signature is also present in
442 interferon-associated inflammation of Trisomy 21 (*77*). In an acutely inflamed environment such as
443 COVID-19, kynurenine is strongly correlated with both IL-6 levels and disease severity (*25, 27, 78*).
444 Notably, comparable damage to RBC membrane lipids and proteins has been documented in COVID-19
445 patients (*79*), in line with decreased RBC deformability (*80, 81*). These studies, however, were performed
446 using blood from one or two collections and thus represented "snapshots" of individual biology at the time
447 of collection. In this study, we were able to obtain a more dynamic view of this network after paired,
448 longitudinal sampling in the same subjects. Collectively, the association between cell rheology and
449 oxidative damage to proteins and lipids reinforces previous findings, though expands these from
450 therapeutic settings such as blood storage and pathological settings such as COVID-19 to a new setting of
451 prolonged endurance exercise.
452 The present findings not only confirm that extreme endurance exercise induces a complex cascade
453 of RBC damage and repair processes, but also offer mechanistic insights that have broader implications.
454 Repeated exposure to mechanical trauma (e.g., foot-strike hemolysis) and additionally circulatory shear
455 stress, compounded by metabolic perturbations, appears to trigger oxidative injury that is evident in the
456 accumulation of oxidized proteins (e.g., methionine oxidation) and altered lipid profiles. In addition to
457 these mechanistic insights, our study underscores important differences between running-based endurance
458 activities and other modalities such as cycling. Running, particularly on hard surfaces and in challenging
459 trail environments, uniquely exacerbates mechanical damage to RBCs through repetitive impact forces.
460 In contrast, non–weight-bearing activities predominantly induce shear stress without the added burden of
461 direct mechanical trauma. This distinction is critical when considering the design of training programs
462 and recovery strategies, as athletes engaged in running sports may require targeted interventions—such as
463 optimized nutritional support (e.g., antioxidants, pantothenate, or carnitine supplementation) or tailored
464 recovery protocols—to minimize RBC damage and maintain optimal oxygen transport capacity.
465 Moreover, the multi-omics signatures identified here have direct implications for athletic
466 performance and recovery. The observed decreases in RBC deformability and alterations in metabolite
467 and protein profiles suggest that prolonged endurance exercise challenges the balance between RBC
468 damage and repair. In the short term, this imbalance may impair microcirculatory flow and reduce oxygen
469 delivery, contributing to performance decline during ultramarathons. Over the longer term, repeated bouts

of exercise-induced RBC turnover could drive hematological adaptations that, while beneficial (e.g., a younger, more resilient RBC pool), also risk cumulative damage if recovery is insufficient. These insights pave the way for future research aimed at defining an "optimal range" of hemolysis and RBC turnover during exercise—a concept that could be instrumental in developing personalized training and nutritional interventions.

Inter-individual variability, driven by factors such as age, sex, training status, and genetic predisposition likely influences the degree of molecular damage observed, highlighting the need for personalized approaches in exercise regimens and recovery strategies. Moreover, the parallels between the molecular signatures observed in endurance athletes and those in other models of oxidative stress—such as sepsis, aging, or even storage lesions in transfused blood—offer broader biological insights that could extend to clinical settings, including transfusion medicine. Finally, while the current study provides a comprehensive snapshot of the acute molecular responses to long-distance running, future longitudinal studies are needed to assess the persistence of these changes and to directly link molecular alterations to functional outcomes. Such work would not only deepen our understanding of exercise-induced cellular stress but also inform interventions aimed at preserving RBCs functionality and overall cardiovascular health in athletes.

Materials and Methods

Sample Collection, Hematological, and Hemorheological Measurements

Sample collection and analyses have been previously described (*14*). Briefly, blood samples were collected from endurance-trained participants before and after either a 40 km trail race (MCC) or a 171 km ultra-trail (UTMB), under similar environmental conditions. Standardized protocols were used to assess hematological, hemorheological, and red blood cell senescence parameters, including blood viscosity, RBC deformability and aggregation, plasma free hemoglobin, microparticle release, phosphatidylserine exposure, and inflammatory markers such as IL-6. Full methodological details have been described previously

Metabolomics and Lipidomics Sample Preparation

Prior to metabolomics or lipidomics analysis, individual samples were placed in 1.5 ml tubes for either metabolite or lipid extraction. Twenty µL were suspended in 180 µL of water/methanol (50:50 v/v) for metabolite extraction or 180 µL of isopropanol/methanol (50:50 v/v) for lipid extraction. Suspensions were vortexed for 30 minutes at 4°C and then centrifuged for 10 minutes, 18,213g, 4°C. Supernatants were isolated for LC-MS.

Metabolomics and Lipidomics UHPLC-MS data acquisition and processing

Analyses were performed as previously published. (*82, 83*) Briefly, the analytical platform employs a Vanquish UHPLC system (Thermo Fisher Scientific, San Jose, CA, USA) coupled online to a Q Exactive mass spectrometer (Thermo Fisher Scientific, San Jose, CA, USA). Polar metabolite extracts are resolved in singlicate over a Kinetex C18 column, 2.1 x 150 mm, 1.7 µm particle size (Phenomenex, Torrance, CA, USA) equipped with a guard column (SecurityGuard™ Ultracartridge – UHPLC C18 for 2.1 mm ID Columns, Phenomenex, Torrance, CA, USA) using an aqueous phase (A) of water and 0.1% formic acid and a mobile phase (B) of acetonitrile and 0.1% formic acid for positive ion polarity mode, and an aqueous phase (A) of water:acetonitrile (95:5) with 1 mM ammonium acetate and a mobile phase (B) of acetonitrile:water (95:5) with 1 mM ammonium acetate for negative ion polarity mode. The column is equilibrated at 5% B, and upon injection of 10 µl of ex-tract, samples are eluted from the column using the solvent gradient: 0.5-1.1 min 5-95% B at 0.45 mL/min; hold at 95% B for 1.65 min at 0.45 mL/min, and then decrease to 5% over 0.25 min at 0.45 ml/min, followed by a re-equilibration hold at 5% B for 2 minutes at 0.45 ml/min. The Q Exactive mass spectrometer (Thermo Fisher Scientific, San Jose, CA, USA) is operated independently in positive or negative ion mode, scanning in Full MS mode (2 µscans)

517 from 60 to 900 m/z at 70,000 resolution, with 4 kV spray voltage, 45 sheath gas, 15 auxiliary gas, AGC
518 target = 3e6, maximum IT = 200 ms. Non-polar lipid extracts are re-solved over an ACQUITY HSS T3
519 column (2.1 x 150 mm, 1.8 µm particle size (Waters, MA, USA) using an aqueous phase (A) of 25%
520 acetonitrile and 5 mM ammonium acetate and a mobile phase (B) of 90% isopropanol, 10% acetonitrile
521 and 5 mM ammonium acetate. The column is equilibrated at 30% B, and upon injection of 10 µl of extract,
522 samples are eluted from the column using the solvent gradient: 0-9 min 30-100% B at 0.325 mL/min; hold
523 at 100% B for 3 min at 0.3 mL/min, and then decrease to 30% over 0.5 min at 0.4 ml/min, followed by a
524 re-equilibration hold at 30% B for 2.5 minutes at 0.4 ml/min. The Q Exactive mass spectrometer (Thermo
525 Fisher) is operated in positive ion mode, scanning in Full MS mode (2 µscans) from 150 to 1500 m/z at
526 70,000 resolution, with 4 kV spray voltage, 45 sheath gas, 15 auxiliary gas. When required, dd-MS2 is
527 performed at 17,500 resolution, AGC target = 1e5, maximum IT = 50 ms, and stepped NCE of 25, 35 for
528 positive mode, and 20, 24, and 28 for negative mode. Calibration is performed prior to analysis using the
529 Pierce™ Positive and Negative Ion Calibration Solutions (Thermo Fisher Scientific).

530 **Metabolomics and Lipidomics Data analysis**

531 Acquired data were converted from raw to mzXML file format using Mass Matrix (Cleveland, OH, USA).
532 Samples were analyzed in randomized order with a technical mixture injected after every 10 samples to
533 qualify instrument performance. Metabolite assignments are performed using accurate intact mass (sub-
534 10 ppm), Isotopologue distributions, and retention time/spectral comparison to an in-house standard
535 compound library (MSMLS, IROA Technologies, NJ, USA) using MAVEN (Princeton, NJ, USA).
536 Lipidomics data are analyzed using LipidSearch 5.0 (Thermo Scientific), which provides lipid
537 identification on the basis of accurate intact mass, isotopic pattern, and fragmentation pattern to determine
538 lipid class and acyl chain composition. Graphs, heat maps and statistical analyses (either T-Test or
539 ANOVA), multivariate analyses including Principal Component Analysis (PCA), Partial Least Squares-
540 Discriminant Analysis (PLS-DA), hierarchical clustering analysis (HCA), and metabolite pathway
541 enrichment analysis are performed using MetaboAnalyst 5.0 (*84*) DSPC IL-6 network filtered by degree
542 (1.5), betweenness (1.0), and correlation ($p < 0.001$) were plotted using CytoScape. (*85*)

543 **Inductively- Coupled Plasma (ICP) Mass Spectrometry**

544 Samples were analyzed as previously published. (*86*) Prior to ICP-MS analysis, 10 µL of plasma were
545 aliquoted into a 15 mL conical tube. 200 µL of 65% nitric acid and 20 ng/mL of gold were added into
546 each sample followed by and addition of 100 µL of 30% hydrogen peroxide and brief vortexing. Samples
547 were then incubated in an oven at 70°C for approximately 2 h. Following incubation, 2190 µL of MilliQ
548 water was added to each tube (final nitric acid percentage of ~5%) and all samples were vortexed briefly.
549 All sam-ples were then diluted 1:15 in a solution consisting of 20 ng/mL and 5% nitric acid. Final dilutions
550 of 1:250 and 1:3750 were then analyzed via ICP-MS. Different dilutions were used to ensure all analytes
551 fell within the calibration curves. All chemicals and materials used for ICP-MS analysis were obtained
552 from Thermo Fisher and all ICP-MS calibrants and solutions were obtained from SPEX CertiPrep. All
553 samples were analyzed on a Ther-mo Scientific iCAP RQ ICP-MS coupled to a ESI SC-4DX FAST
554 autosampler system utiliz-ing a peristaltic pump. The optimization of the system was performed before
555 the run by first calibrating the system with ICP-MS iCAP Q/Qnova Calibration Solution, Specpure. The
556 system was subsequently tuned using a tuning solution consisting of Ba, Bi, Ce, Co, In, Li, and U at 1.00
557 ± 0.05 µg/L. To monitor performance while the system was running, we continually pumped internal
558 standard mix via the peristaltic pump and monitored signal throughout the run. Additionally, quality
559 controls of a known concentration of each analyte were injected at the beginning, throughout the run
560 between samples, and at the end of the run. Acceptance criteria for all QCs was ±25% of the known
561 concentration. Thermo Scientific Qtegra software was used for all data acquisition and analysis.

562 **Proteomics Sample Preparation**

Plasma and RBC samples were digested using S-Trap 96-well plates (Protifi, Huntington, NY) following the manufacturer's protocol. Briefly, approximately 50 µg of protein was mixed with 5% SDS. Samples were reduced with 10 mM dithiothreitol (DTT) at 55°C for 30 minutes, cooled to room temperature, and alkylated with 25 mM iodoacetamide (IAM) in the dark for 30 minutes.Next, phosphoric acid was added to achieve a final concentration of 2.5 % followed by six volumes of binding buffer (90% methanol, 100 mM triethylammonium bicarbonate [TEAB], pH 7.1). After gentle mixing, the protein solution was loaded onto an S-Trap 96-well plate and centrifuged at 1500 × g for 2 minutes. The plate was then washed three times with 300 µL of binding buffer. For digestion, 1 µg of sequencing-grade trypsin (Promega) and 125 µL of digestion buffer (50 mM TEAB) were added to the filter, and samples were incubated at 37°C for 6 hours. Peptides were sequentially eluted using 100 µL of each of the following buffers: (1) 50 mM TEAB, (2) 0.2% formic acid in water, and (3) 50% acetonitrile with 0.2% formic acid in water. The peptide solutions were pooled, lyophilized, and resuspended in 500 µL of 0.1% formic acid (FA)

Proteomics Data acquisition and processing

A 20 µL aliquot of each sample was loaded onto individual Evotips for desalting, followed by three washes with 200 µL of 0.1% formic acid (FA). To maintain hydration until analysis, 100 µL of storage solvent (0.1% FA) was added to each Evotip. Peptide separation was performed using a PepSep column (150 µm inner diameter, 15 cm) packed with ReproSil C18 (1.9 µm, 120Å resin) and a pre-set 30 samples-per-day gradient on the Evosep One system (Evosep, Odense, Denmark). The Evosep One system was coupled to a timsTOF Pro mass spectrometer (Bruker Daltonics, Bremen, Germany) via a CaptiveSpray nano-electrospray ion source (Bruker Daltonics). The mass spectrometer was operated in DIA-PASEF mode. We used a method with four windows in each 100 ms dia-PASEF scan. 32 of these scans covered the diagonal scan line for doubly and triply charged peptides in the m/z - ion mobility plane with narrow 25 m/z precursor windows.

A project specific spectral library generated from 24 high-pH reverse-phase peptide fractions acquired with DDA-PASEF acquisition. MS data were collected over an m/z range of 100 to 1,700. During each MS/MS data collection, each TIMS cycle was 1.17 seconds and included 1 MS and 10 PASEF MS/MS scans. Low-abundance precursor ions with an intensity above a threshold of 500 counts but below a target value of 20000 counts were repeatedly scheduled and otherwise dynamically excluded for 0.4 min. Pooled plasma or RBCs digest was separated by high pH reversed phase chromatography on a Gemini-NH C18, 4.6 x 250 mm analytical column containing 3 µM particles, flow rate was 0.6 mL/min. The solvent consisted of 20 mM ammonium bicarbonate (pH 10) as mobile phase (A) and 20 mM ammonium bicarbonate and 75% ACN (pH 10) as mobile-phase B. Sample separation was accomplished using the following linear gradient: from 0 to 5% B in 10 min, from 5 to 50% B in 80 min, from 50 to 100% B in 10 min, and held at 100% B for an additional 10 min. 96 fractions were collected along with the LC separation and were concatenated into 24 fractions by combining fractions 1, 25, 49, 73 and so on. Samples were dried in Speed-Vac, resuspended in 80 ul of 0.1% FA and 20ul of each fraction was loaded onto individual Evotips.

Proteomics Data Processing

Raw .d files were analyzed with Spectronaut 17.6 (Biognosys) using default settings (*87*). Spectral libraries were prepared searching for carbamidomethyl (C), Glu>PyroGlu, and Acetyl (N-ter) as fixed modifications, with variable modifications including methyl (D,E), deamidation (N), oxidation (M), His>Asp, Phospho (ST), oxidation (W), dioxidation, and GlyGly (K). Proteomics GO networks were prepared using ShinyGO 0.82 (*88, 89*)

Acknowledgments

Funding: A.D. was supported by funds from the NHLBI, National Institutes of Health (R01HL146442). The content is solely the responsibility of the authors and does not necessarily represent the official views of the National Institutes of Health.

Author contributions:

Conceptualization: PC, AD
Methodology: TN, FC, DS, MD
Investigation: TN, ES, FC,EN, MR, SS, PR, GM, PC, DS, MD
Visualization: TN
Supervision: PC, AD, TN, KCH
Writing—original draft: TN, AD
Writing—review & editing: All authors

Competing interests: A.D., K.C.H., and T.N. are founders of Omix Technologies Inc. A.D. and T.N. are scientific advisory board members for Hemanext Inc. A.D. is a scientific advisory board member for Macopharma Inc. The remaining authors declare no competing financial interests.

Data and materials availability: All data are available in the main text or the supplementary materials.

Figures and Tables

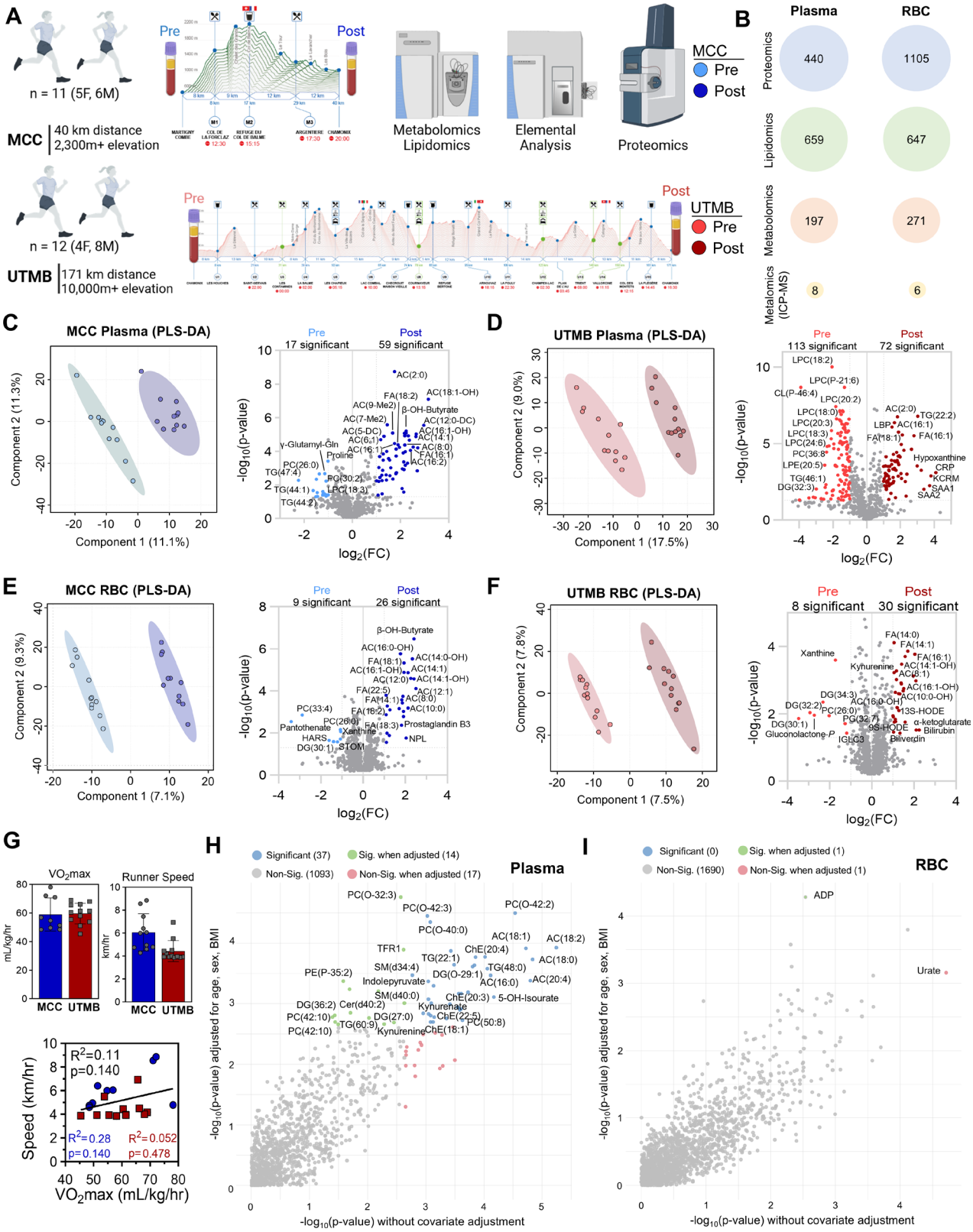

Figure 1 Multiomics of a 40 km or 171 km Run. (A) Plasma and RBC were taken before (Pre) and after (Post) a 40-km (Martigny–Combes à Chamonix race, MCC) or 141-km (Ultra-Trail du Mont Blanc, UTMB©) footrace. (B) Proteomics, lipidomics, metabolomics using liquid

chromatography mass spectrometry (LC-MS), and metalomics using ion coupled plasmon (ICP)-MS were collected. Processed data contained measurements for the number of analytes shown in the respective circle for each fraction. (C) Partial Least Squares Discriminant Analysis (PLS-DA) of the plasma fraction during the MCC and (D) UTMB along with associated volcano plots highlighting all analytes with fold change (FC) > 1.5 and p-value < 0.05 from a paired T-test. (E) PLS-DA of the RBC fraction during the MCC and (F) UTMB along with associated volcano plots highlighting all analytes with fold change (FC) > 1.5 and p-value < 0.05 from a paired T-test. (G) VO_2max and speed for all runners in each race. A Pearson correlation between the two measurements for both races is shown in black. R2 and p-values for each race are also shown in the respective colors. (H) Linear mixed model adjusted for age, sex, BMI of runner speed (km/hr) in the plasma, or (I) RBC fraction.

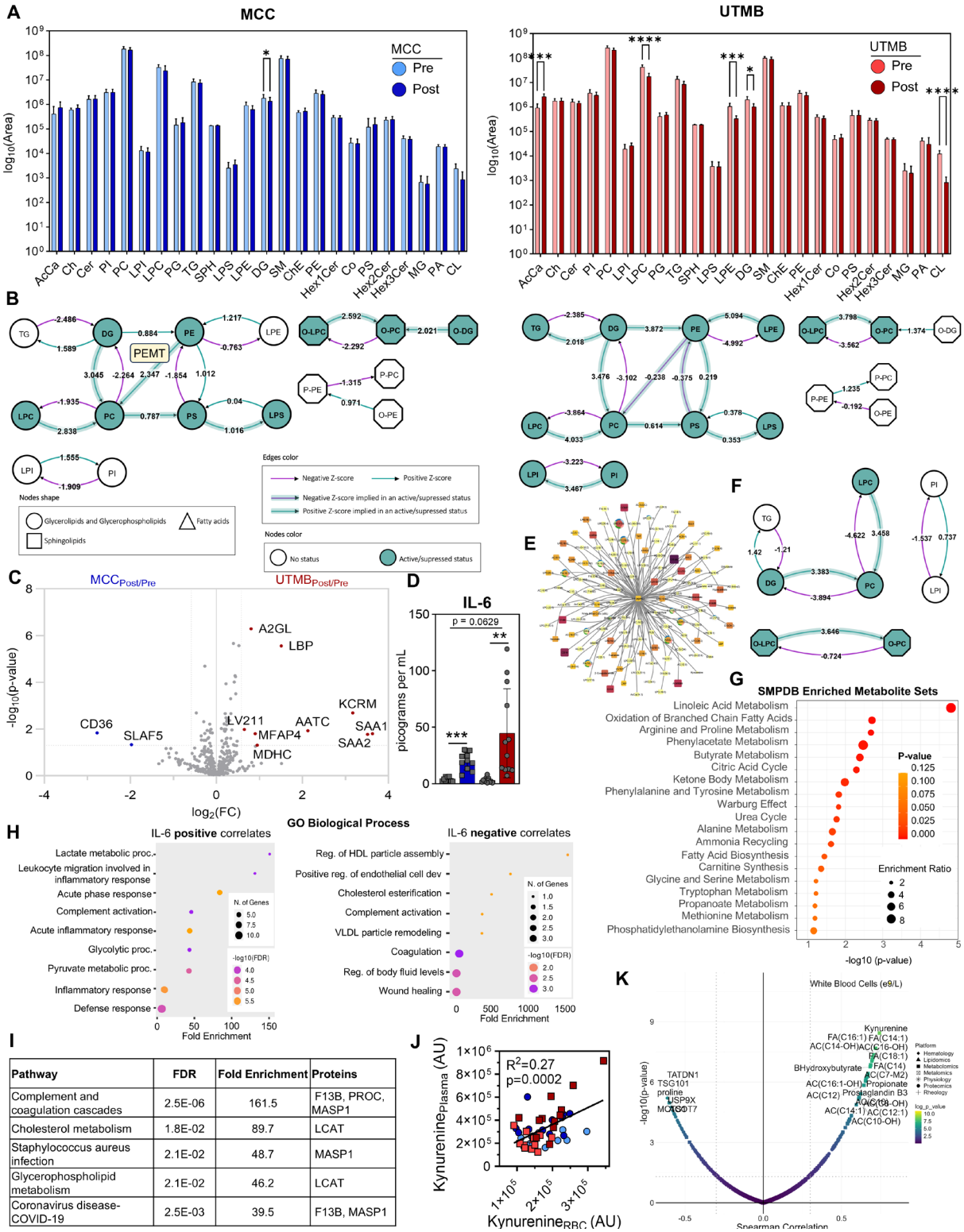

Pathway	FDR	Fold Enrichment	Proteins
Complement and coagulation cascades	2.5E-06	161.5	F13B, PROC, MASP1
Cholesterol metabolism	1.8E-02	89.7	LCAT
Staphylococcus aureus infection	2.1E-02	48.7	MASP1
Glycerophospholipid metabolism	2.1E-02	46.2	LCAT
Coronavirus disease-COVID-19	2.5E-03	39.5	F13B, MASP1

Figure 2 Lipidomics of the MCC and UTMB. (A) Total lipid class quantities shown as $\log_{10}$(Peak area sum) before and after the MCC and UTMB. (B) BioPAN models of lipid class flux during the MCC (left) and UTMB (right). Lipid classes are indicated by node shape where filled nodes indicate significantly modified class. Fluxes normalized by Z-score with positive fluxes shown in teal and negative fluxes shown in purple. (C) A volcano plot showing the intra-subject proteomic fold changes with respect to each race. (D) IL-6 measurements before and after the

MCC (blue) and UTMB (red). (E) A Debiased Sparse Partial Correlation (DSPC) network of IL-6. (F) BioPAN model of lipid pathway flux for lipids significantly associated with IL-6 levels. (G) Metabolite set enrichment analysis for metabolites lipids significantly associated with IL-6 levels. (H) Gene Ontology analyses for proteins positively (left) of negatively (right) significantly associated with IL-6 levels. (I) KEGG pathway enrichment based on proteomics data. (J) Kynurenine correlations between plasma (y-axis) and RBC (x-axis) compartment. (K) RBC molecular correlates with plasma IL-6 levels.

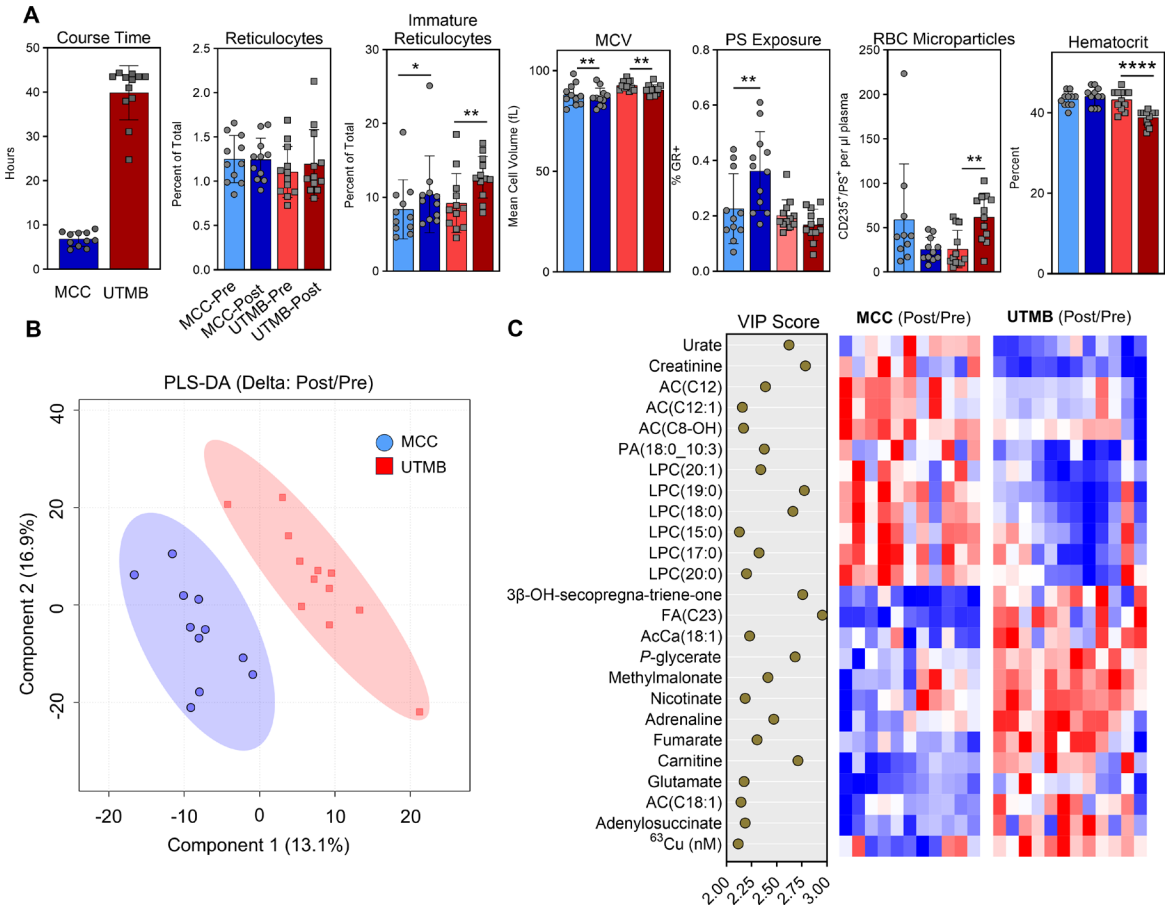

Figure 3 RBC Multiomics of Running. (A) Hematologic parameters of each race is shown. (B) PLS-DA of intra-subject normalized molecular values for each race. (C) The top 25 molecules based on Variable Importance in Projection (VIP) for the PLS-DA are shown (left) along with relative values of intra-subject fold changes for each race in the heat map (right).

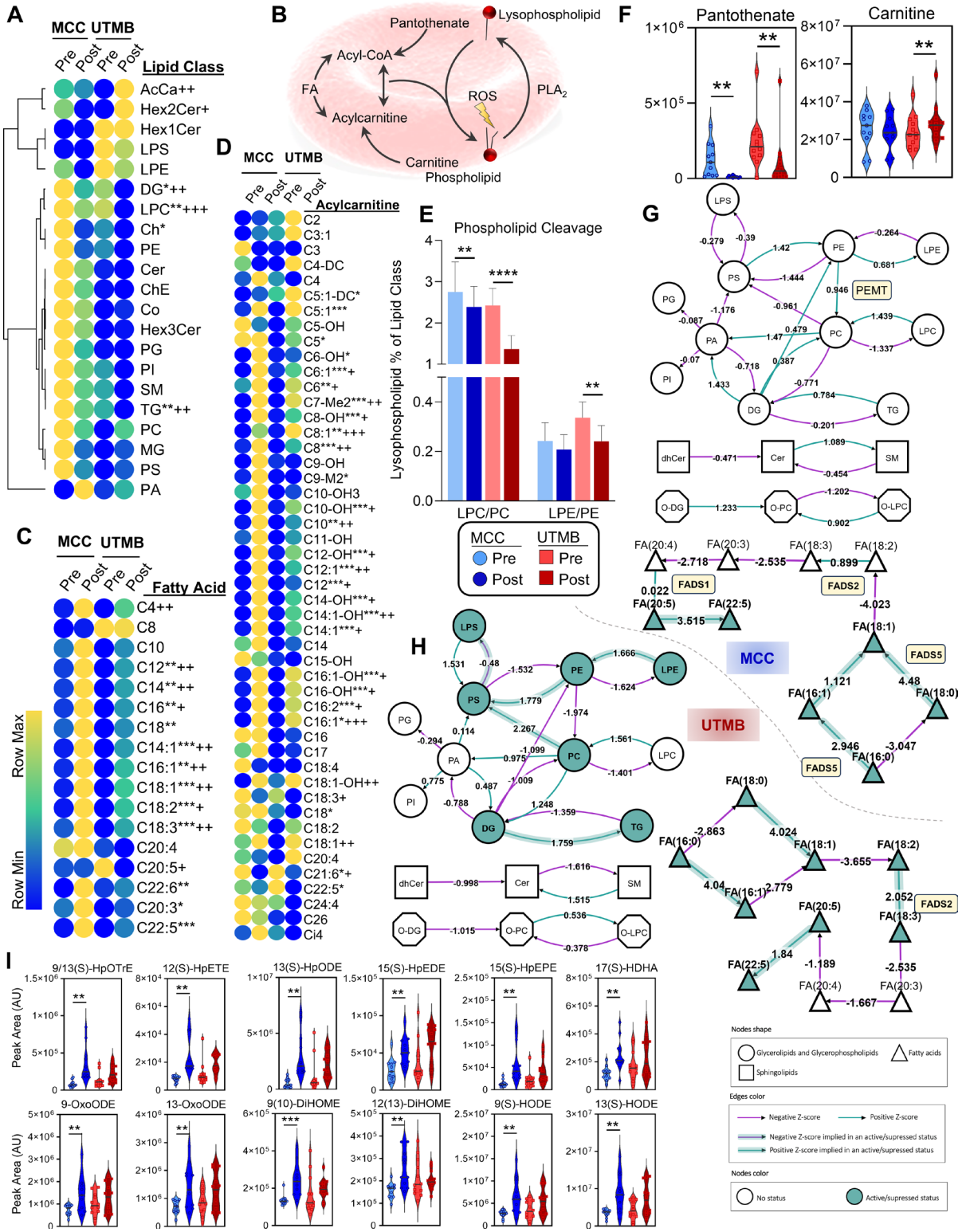

Figure 4 RBC Lipidomics. (A) The average peak areas of lipids identified from untargeted analysis were summed according to lipid class and plotted as a heat map. p-values from Two-tailed paired T-test for MCC pre/post comparisons are indicated as *, p<0.05; **, p<0.01, ***, p<0.001; ****, p<0.0001 and p-values for UTMB pre/post comparisons are indicated as +, p<0.05; ++, p<0.01, +++, p<0.001; ++++, p<0.0001. (B) A cartoon of the Lands cycle for red blood cell membrane repair is shown. (C) Average peaks areas from semi-targeted analysis for fatty acids

and (D) acylcarnitines are shown as heat maps. (E) The ratio of lysophospholipid-to-phospholipid by group from untargeted analysis (F) The levels of pantothenate and carnitine are plotted as violin plots. (G) BioPAN or RBC during the MCC and (H) UTMB are shown. (I) Violin plots of significant oxylipins before and after the MCC (blue) and UTMB (red).

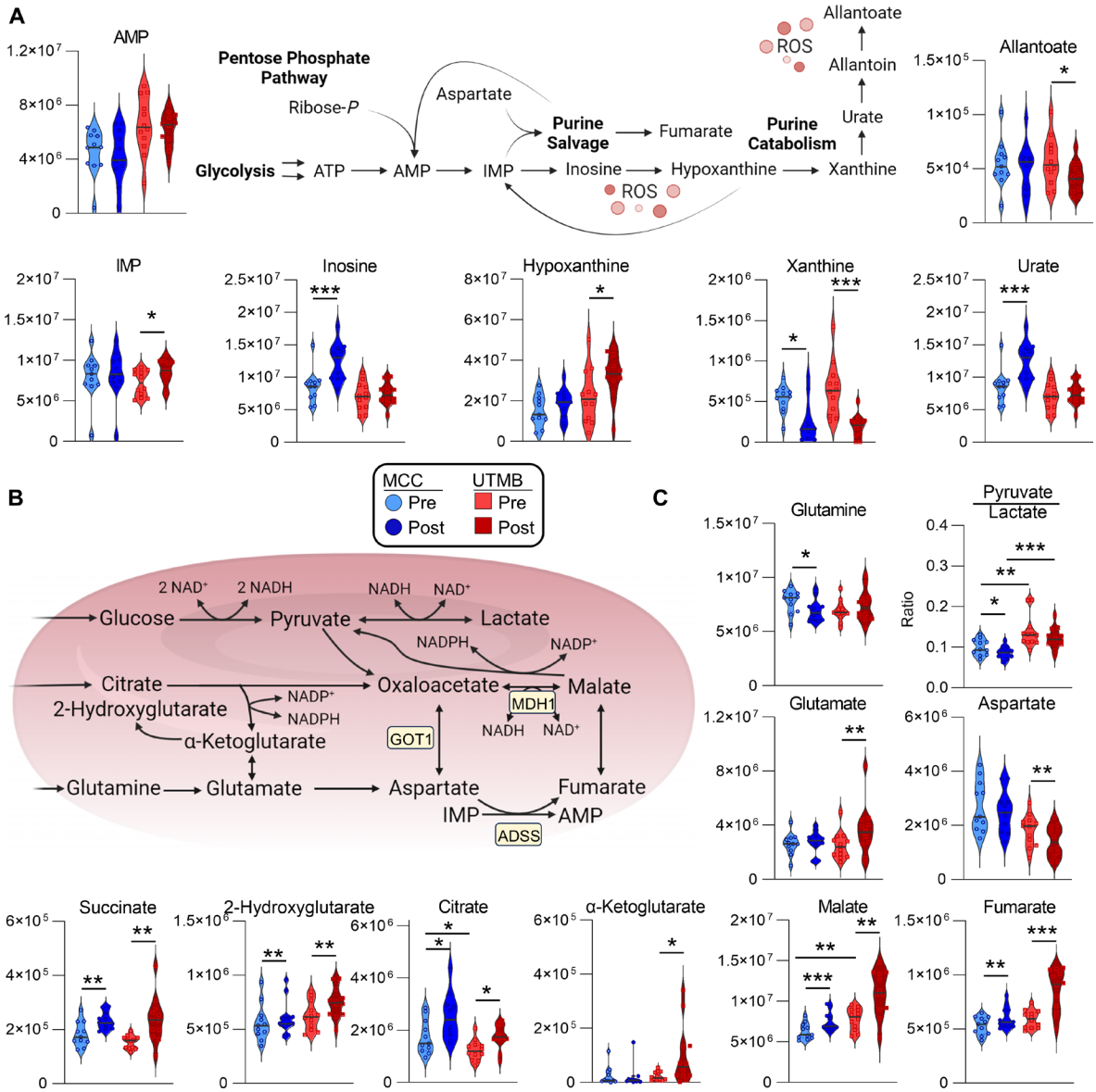

Figure 5 Purine Salvage and Carboxylate Metabolism in RBC. Metabolites in the (A) purine salvage or (B) carboxylate metabolism pathways are shown. Individual samples from MCC (O) at Pre (light blue) and Post (dark blue), or UTMB (□) at Pre (light red) or Post (dark red) are shown within violin plots. p-values from Two-tailed homoscedastic T-tests are indicated as *, p<0.05; **, p<0.01, ***, p<0.001; ****, p<0.0001. The pathway map (center) was created with Biorender.com.

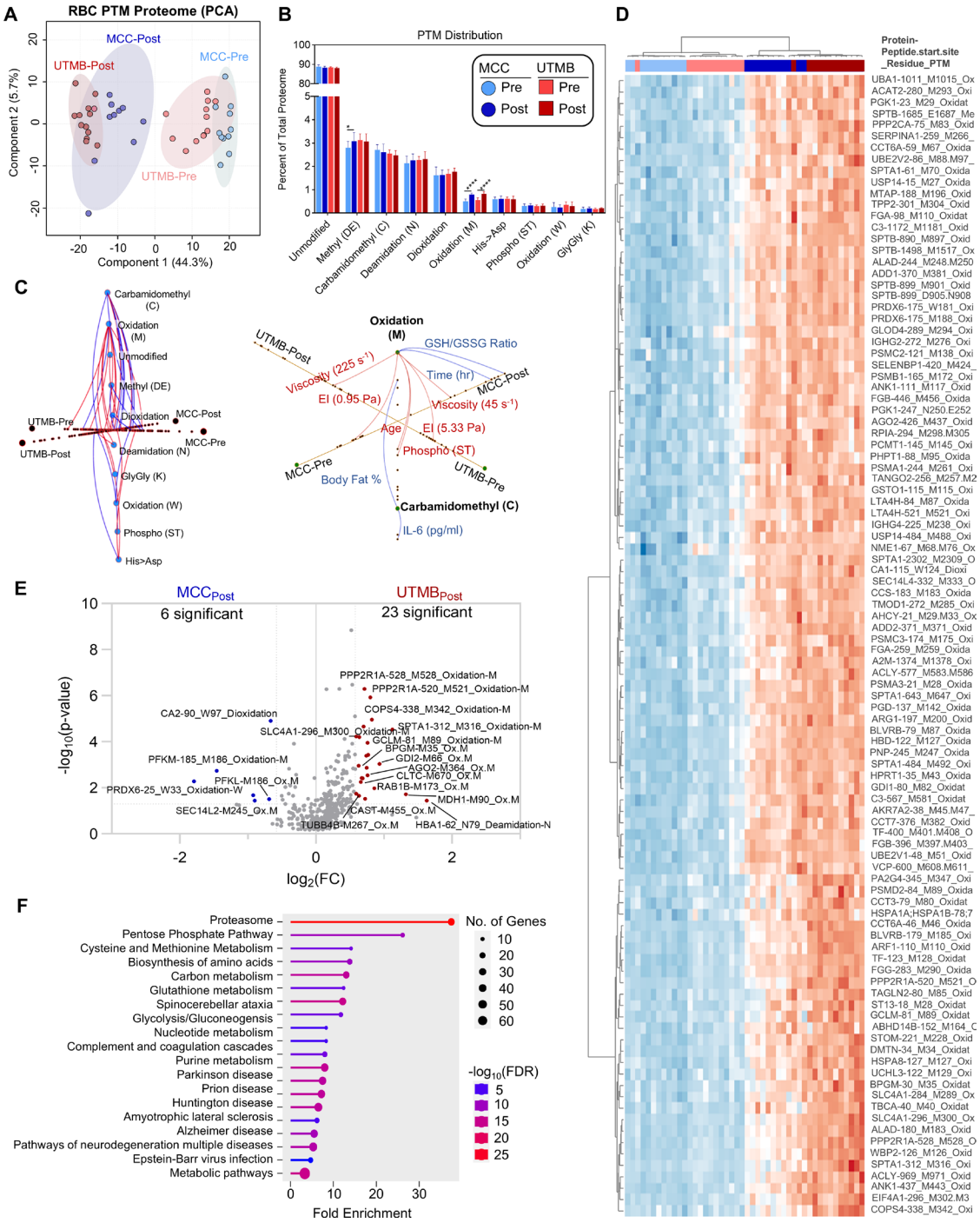

Figure 6 RBC Proteomics demonstrates increased protein oxidation. (A) Principal Component Analysis (PCA) of RBC peptide-level data. (B) Distribution of post translational modification (PTM) across the proteome. (C) Hive plot of significant Pearson correlations (R) between physiological, hematological, and rheological parameters are shown with R > 0.7 shown in red and R < -0.7 shown in blue. On the right, a labeled plot showing Pearson correlations (R > 0.7, R < -0.7) with methionine oxidation and cysteine carbamidomethylation. (D) Heat map showing relative peptide abundance across MCC and UTMB. (E) Volcano plot comparing peptide levels in the post MCC and UTMB samples. (F) KEGG Pathway enrichment of proteins with statistically significant (ANOVA Fisher's LSD FDR < 0.05) enrichment of methionine oxidation.

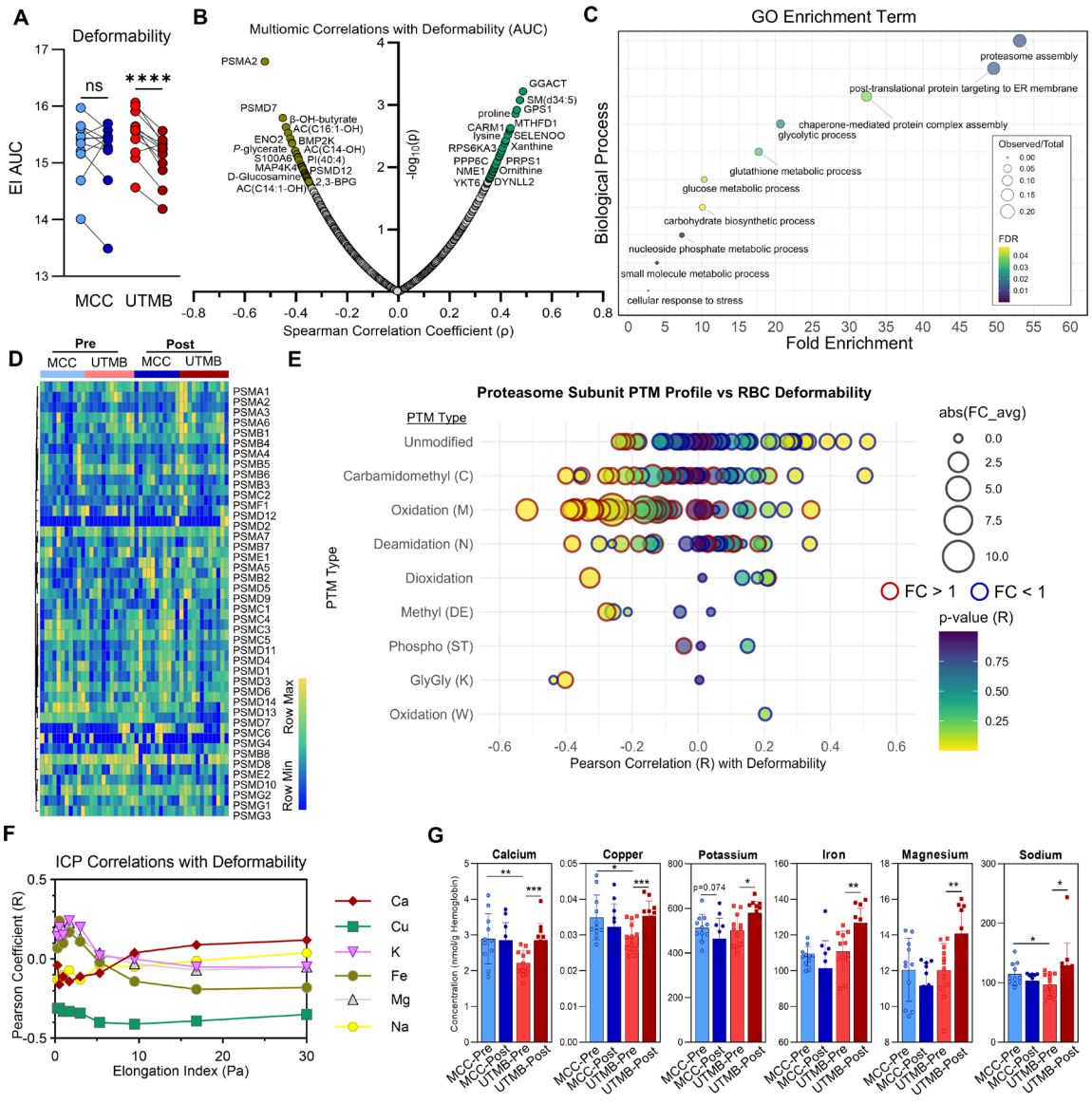

Figure 7 Molecular Correlates with RBC Deformability. A) Total deformability decreases specifically after UTMB (see Sup Fig for deform on all Pressures). B) Spearman correlations with Deformability AUC. C) GO Enrichment terms with deformability. D) Heatmap showing total levels of proteasome subunits. (E) Dot plot showing the Pearson correlation with RBC deformability on the x-axis. The size of each dot is proportional to the Post/Pre fold change and the dot outline indicates with the fold change increased (red) or decreased (blue) after the race. The significance of the correlation is indicated by color. (F) Pearson correlation at each shear stress pressure for metals, along with (G) abundance before and after each race.

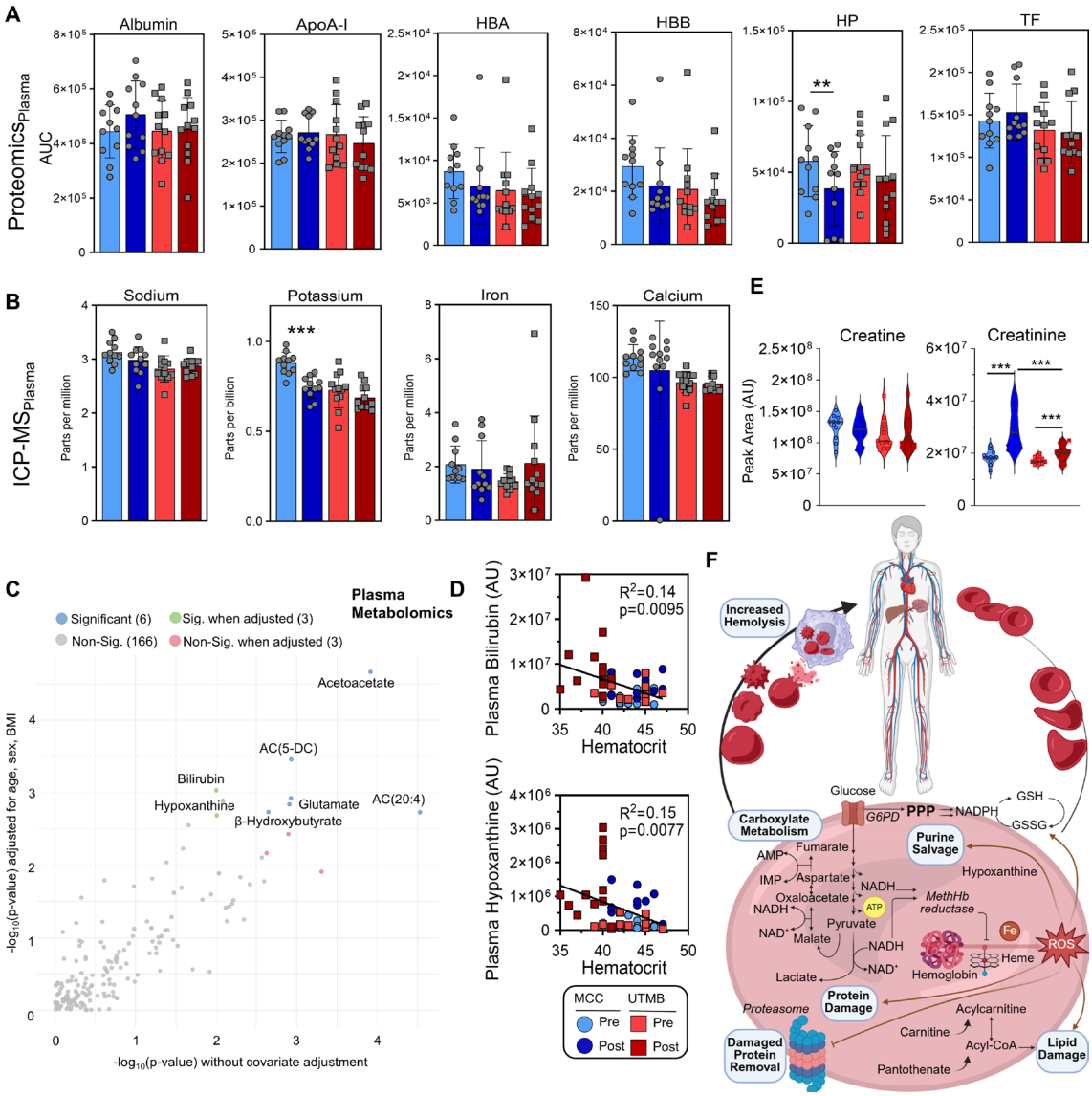

Figure 8 Multi-Omics signatures in plasma highlight increased hemolysis after ultrarunning. (A) The plasma levels of abundant proteins albumin, apolipoprotein A1 (ApoA-I), hemoglobin alpha (HBA) and beta (HBB), haptoglobin (HP), and transferrin (TF). (B) Plasma levels of trace elements. (C) Linear mixed model of hematocrit corrected for age, sex, height, and weight using plasma metabolomics data. (D) Pearson correlation plots of hematocrit and plasma levels of bilirubin and hypoxanthine. Individual races and time points are indicated. (E) RBC levels of creatine and creatinine. (F) A proposed model of RBC damage accumulation during long distance trail running.

Supplementary Materials

Supplementary materials are provided as 5 Tables (spreadsheet xlsx format) and 7 figures (pdf).

References

1. H. Mairbäurl, Red blood cells in sports: effects of exercise and training on oxygen supply by red blood cells. *Frontiers in Physiology* **4**, 332 (2013).
2. T. Yoshida, M. Prudent, A. D'Alessandro, Red blood cell storage lesion: causes and potential clinical consequences. *Blood Transfusion*, (2019).
3. A. D'Alessandro, K. C. Hansen, E. Z. Eisenmesser, J. C. Zimring, Protect, repair, destroy or sacrifice: a role of oxidative stress biology in inter-donor variability of blood storage? *Blood Transfus* **17**, 281-288 (2019).
4. M. Hargreaves, L. L. Spriet, Skeletal muscle energy metabolism during exercise. *Nat Metab* **2**, 817-828 (2020).
5. S. Amatori *et al.*, Are pre-race serum blood biomarkers associated with the 24-h ultramarathon race performance? *European Journal of Sport Science* **24**, 431-439 (2024).
6. A. Siekierzycka *et al.*, Plasma cardiovascular stress biomarkers response to marathon running. *Sports Medicine and Health Science*, (2024).
7. T. Nemkov *et al.*, Acute Cycling Exercise Induces Changes in Red Blood Cell Deformability and Membrane Lipid Remodeling. *Int J Mol Sci* **22**, (2021).
8. I. San-Millán *et al.*, Metabolomics of Endurance Capacity in World Tour Professional Cyclists. *Frontiers in Physiology* **11**, 578 (2020).
9. R. Fleischer, Ueber eine neue form von haemoglobinurie beim menschen. *Berl Klin Wschr* **18**, 691 (1881).
10. A. Gartner, N. Dombrowski, N. Lowe, V. Behzadpour, R. Zackula, Foot-strike Hemolysis: A Scoping Review of Long-Distance Runners. *Kans J Med* **17**, 119-124 (2024).
11. D. Nash *et al.*, IL-6 signaling in acute exercise and chronic training: Potential consequences for health and athletic performance. *Scand J Med Sci Sports* **33**, 4-19 (2023).
12. H. Northoff, A. Berg, Immunologic mediators as parameters of the reaction to strenuous exercise. *Int J Sports Med* **12 Suppl 1**, S9-15 (1991).
13. E. Nader *et al.*, Impact of a 10 km running trial on eryptosis, red blood cell rheology, and electrophysiology in endurance trained athletes: a pilot study. *European Journal of Applied Physiology* **120**, 255-266 (2020).
14. M. Robert *et al.*, Impact of Trail Running Races on Blood Viscosity and Its Determinants: Effects of Distance. *Int J Mol Sci* **21**, (2020).
15. S. Skinner *et al.*, Differential impacts of trail and ultra-trail running on cytokine profiles: An observational study. *Clin Hemorheol Microcirc* **78**, 301-310 (2021).
16. K. Contrepois *et al.*, Molecular Choreography of Acute Exercise. *Cell* **181**, 1112-1130.e1116 (2020).
17. C. C. F. Howe *et al.*, Untargeted Metabolomics Profiling of an 80.5 km Simulated Treadmill Ultramarathon. *Metabolites* **8**, (2018).
18. Z. Stander *et al.*, The unaided recovery of marathon-induced serum metabolome alterations. *Sci Rep* **10**, 11060 (2020).
19. T. B. Høeg, K. Chmiel, A. E. Warrick, S. L. Taylor, R. H. Weiss, Ultramarathon Plasma Metabolomics: Phosphatidylcholine Levels Associated with Running Performance. *Sports (Basel)* **8**, (2020).
20. H. Mairbäurl, Red blood cells in sports: Effects of exercise and training on oxygen supply by red blood cells. *Frontiers in Physiology* **4**, (2013).
21. C. Gaud *et al.*, BioPAN: a web-based tool to explore mammalian lipidome metabolic pathways on LIPID MAPS. *F1000Res* **10**, 4 (2021).
22. Y. Chen, J. Zhang, W. Cui, R. L. Silverstein, CD36, a signaling receptor and fatty acid transporter that regulates immune cell metabolism and fate. *J Exp Med* **219**, (2022).

23. T. G. Manfredi *et al.*, Plasma creatine kinase activity and exercise-induced muscle damage in older men. *Med Sci Sports Exerc* **23**, 1028-1034 (1991).
24. S. Basu *et al.*, Sparse network modeling and metscape-based visualization methods for the analysis of large-scale metabolomics data. *Bioinformatics* **33**, 1545-1553 (2017).
25. D. A. Bizjak *et al.*, Kynurenine serves as useful biomarker in acute, Long- and Post-COVID-19 diagnostics. *Front Immunol* **13**, 1004545 (2022).
26. J. P. Dewulf *et al.*, Urine metabolomics links dysregulation of the tryptophan-kynurenine pathway to inflammation and severity of COVID-19. *Sci Rep* **12**, 9959 (2022).
27. T. Thomas *et al.*, COVID-19 infection alters kynurenine and fatty acid metabolism, correlating with IL-6 levels and renal status. *JCI Insight* **5**, (2020).
28. T. Nemkov *et al.*, Regulation of kynurenine metabolism by blood donor genetics and biology impacts red cell hemolysis in vitro and in vivo. *Blood* **143**, 456-472 (2024).
29. E. Nader *et al.*, Eryptosis and hemorheological responses to maximal exercise in athletes: Comparison between running and cycling. *Scandinavian Journal of Medicine & Science in Sports* **28**, 1532-1540 (2018).
30. E. Lang, F. Lang, Triggers, Inhibitors, Mechanisms, and Significance of Eryptosis: The Suicidal Erythrocyte Death. *BioMed Research International* **2015**, 1-16 (2015).
31. T. Nemkov, S. M. Qadri, W. P. Sheffield, A. D'Alessandro, Decoding the metabolic landscape of pathophysiological stress-induced cell death in anucleate red blood cells. *Blood Transfusion*, (2020).
32. A. D'Alessandro *et al.*, Ferroptosis regulates hemolysis in stored murine and human red blood cells. *Blood* **145**, 765-783 (2025).
33. M. A. Perez *et al.*, Ether lipid deficiency disrupts lipid homeostasis leading to ferroptosis sensitivity. *PLoS Genet* **18**, e1010436 (2022).
34. T. Thomas *et al.*, Fatty acid desaturase activity in mature red blood cells and implications for blood storage quality. *Transfusion*, (2021).
35. A. D'Alessandro *et al.*, Functional and multi-omics signatures of mitapivat efficacy upon activation of pyruvate kinase in red blood cells from patients with sickle cell disease. *Haematologica* **109**, 2639-2652 (2024).
36. T. Nemkov *et al.*, Hypoxia modulates the purine salvage pathway and decreases red blood cell and supernatant levels of hypoxanthine during refrigerated storage. *Haematologica* **103**, 361-372 (2018).
37. C. Chen *et al.*, Erythrocyte ENT1-AMPD3 Axis is an Essential Purinergic Hypoxia Sensor and Energy Regulator Combating CKD in a Mouse Model. *J Am Soc Nephrol* **34**, 1647-1671 (2023).
38. T. Nemkov *et al.*, Metabolism of Citrate and Other Carboxylic Acids in Erythrocytes As a Function of Oxygen Saturation and Refrigerated Storage. *Frontiers in Medicine* **4**, 175 (2017).
39. A. D'Alessandro *et al.*, Donor sex, age and ethnicity impact stored red blood cell antioxidant metabolism through mechanisms in part explained by glucose 6-phosphate dehydrogenase levels and activity. *Haematologica*, haematol.2020.246603 (2020).
40. R. O. Francis *et al.*, Donor glucose-6-phosphate dehydrogenase deficiency decreases blood quality for transfusion. *J Clin Invest* **130**, 2270-2285 (2020).
41. S. Peltier *et al.*, Proteostasis and metabolic dysfunction characterize a subset of storage-induced senescent erythrocytes targeted for post-transfusion clearance. *J Clin Invest*, (2025).
42. J. A. Reisz *et al.*, Methylation of protein aspartates and deamidated asparagines as a function of blood bank storage and oxidative stress in human red blood cells. *Transfusion* **58**, 2978-2991 (2018).
43. Z. Lv *et al.*, Domain alternation and active site remodeling are conserved structural features of ubiquitin E1. *J Biol Chem* **292**, 12089-12099 (2017).

820 44. F. Rapido *et al.*, Prolonged red cell storage before transfusion increases extravascular hemolysis.
821 *J Clin Invest* **127**, 375-382 (2017).
822 45. G. Lippi, M. Plebani, S. Di Somma, G. Cervellin, Hemolyzed specimens: a major challenge for
823 emergency departments and clinical laboratories. *Crit Rev Clin Lab Sci* **48**, 143-153 (2011).
824 46. I. Syllm-Rapoport, A. Daniel, H. Starck, A. Hartwig, J. Gross, Creatine in density-fractionated
825 red cells, a useful indicator of erythropoietic dynamics and of hypoxia past and present. *Acta*
826 *Haematol* **66**, 86-95 (1981).
827 47. C. P. Ku, H. Passow, Creatine and creatinine transport in old and young human red blood cells.
828 *Biochim Biophys Acta* **600**, 212-227 (1980).
829 48. F. E. Boas, L. Forman, E. Beutler, Phosphatidylserine exposure and red cell viability in red cell
830 aging and in hemolytic anemia. *Proc Natl Acad Sci U S A* **95**, 3077-3081 (1998).
831 49. D. Montero, C. Lundby, Regulation of Red Blood Cell Volume with Exercise Training. *Compr*
832 *Physiol* **9**, 149-164 (2018).
833 50. T. R. Klei, S. M. Meinderts, T. K. van den Berg, R. van Bruggen, From the Cradle to the Grave:
834 The Role of Macrophages in Erythropoiesis and Erythrophagocytosis. *Front Immunol* **8**, 73
835 (2017).
836 51. R. D. Telford *et al.*, Footstrike is the major cause of hemolysis during running. *J Appl Physiol*
837 *(1985)* **94**, 38-42 (2003).
838 52. T. Yamada, M. Tohori, T. Ashida, N. Kajiwara, H. Yoshimura, Comparison of effects of
839 vegetable protein diet and animal protein diet on the initiation of anemia during vigorous
840 physical training (sports anemia) in dogs and rats. *J Nutr Sci Vitaminol (Tokyo)* **33**, 129-149
841 (1987).
842 53. R. Beneke, D. Bihn, M. Hütler, R. M. Leithäuser, Haemolysis caused by alterations of alpha- and
843 beta-spectrin after 10 to 35 min of severe exercise. *Eur J Appl Physiol* **95**, 307-312 (2005).
844 54. A. Yusof *et al.*, Exercise-induced hemolysis is caused by protein modification and most evident
845 during the early phase of an ultraendurance race. *J Appl Physiol (1985)* **102**, 582-586 (2007).
846 55. J. A. Smith, Exercise, Training and Red Blood Cell Turnover:. *Sports Medicine* **19**, 9-31 (1995).
847 56. O. S. Platt, S. E. Lux, D. G. Nathan, Exercise-induced hemolysis in xerocytosis. Erythrocyte
848 dehydration and shear sensitivity. *J Clin Invest* **68**, 631-638 (1981).
849 57. W. van Beaumont, S. Underkofler, S. van Beaumont, Erythrocyte volume, plasma volume, and
850 acid-base changes in exercise and heat dehydration. *Journal of Applied Physiology* **50**, 1255-
851 1262 (1981).
852 58. V. Lipovac, M. Gavella, Z. Turk, Z. Škrabalo, Influence of lactate on the insulin action on red
853 blood cell filterability. *Clinical Hemorheology and Microcirculation* **5**, 421-428 (2016).
854 59. J. A. Smith, R. D. Telford, M. Kolbuch-Braddon, M. J. Weidemann, Lactate/H+ uptake by red
855 blood cells during exercise alters their physical properties. *European Journal of Applied*
856 *Physiology and Occupational Physiology* **75**, 54-61 (1997).
857 60. P. Connes *et al.*, Opposite effects of in vitro lactate on erythrocyte deformability in athletes and
858 untrained subjects. *Clinical Hemorheology and Microcirculation* **31**, 311-318 (2004).
859 61. W. E. Lands, Metabolism of glycerolipides; a comparison of lecithin and triglyceride synthesis.
860 *The Journal of Biological Chemistry* **231**, 883-888 (1958).
861 62. A. Arduini *et al.*, Role of carnitine and carnitine palmitoyltransferase as integral components of
862 the pathway for membrane phospholipid fatty acid turnover in intact human erythrocytes. *The*
863 *Journal of Biological Chemistry* **267**, 12673-12681 (1992).
864 63. A. Arduini *et al.*, Effect of L-carnitine and acetyl-L-carnitine on the human erythrocyte
865 membrane stability and deformability. *Life Sciences* **47**, 2395-2400 (1990).
866 64. A. Arduini *et al.*, Acyl-trafficking in membrane phospholipid fatty acid turnover: The transfer of
867 fatty acid from the acyl-L-carnitine pool to membrane phospholipids in intact human
868 erythrocytes. *Biochemical and Biophysical Research Communications* **187**, 353-358 (1992).

869 65. T. Nemkov *et al.*, Genetic regulation of carnitine metabolism controls lipid damage repair and
870 aging RBC hemolysis in vivo and in vitro. *Blood*, (2024).
871 66. K. F. Annous, W. O. Song, Pantothenic acid uptake and metabolism by red blood cells of rats.
872 *The Journal of Nutrition* **125**, 2586-2593 (1995).
873 67. S. A. Mian *et al.*, Vitamin B5 and succinyl-CoA improve ineffective erythropoiesis in SF3B1-
874 mutated myelodysplasia. *Sci Transl Med* **15**, eabn5135 (2023).
875 68. M. H. Williams, Vitamin supplementation and athletic performance. *International Journal for*
876 *Vitamin and Nutrition Research. Supplement = Internationale Zeitschrift Fur Vitamin- Und*
877 *Ernahrungsforschung. Supplement* **30**, 163-191 (1989).
878 69. M. J. Webster, Physiological and performance responses to supplementation with thiamin and
879 pantothenic acid derivatives. *European Journal of Applied Physiology* **77**, 486-491 (1998).
880 70. L. M. Forbes *et al.*, Red Blood Cell Metabolic Responses during Acute Hypoxic Exercise in
881 Healthy Adults. *Am J Respir Cell Mol Biol* **72**, 456-459 (2025).
882 71. A. A. Barber, F. Bernheim, Lipid peroxidation: its measurement, occurrence, and significance in
883 animal tissues. *Adv Gerontol Res* **2**, 355-403 (1967).
884 72. W. Kim *et al.*, Polyunsaturated Fatty Acid Desaturation Is a Mechanism for Glycolytic NAD(+)
885 Recycling. *Cell Metab* **29**, 856-870.e857 (2019).
886 73. A. Shenkin, Trace elements and inflammatory response: implications for nutritional support.
887 *Nutrition* **11**, 100-105 (1995).
888 74. K. F. Adams, G. Johnson, Jr., K. E. Hornowski, T. H. Lineberger, The effect of copper on
889 erythrocyte deformability: a possible mechanism of hemolysis in acute copper intoxication.
890 *Biochim Biophys Acta* **550**, 279-287 (1979).
891 75. B. O. Adele *et al.*, Alterations in plasma and erythrocyte membrane fatty acid composition
892 following exposure to toxic copper level affect membrane deformability and fluidity in female
893 wistar rats. *J Trace Elem Med Biol* **80**, 127316 (2023).
894 76. H. Li *et al.*, Mechanics of diseased red blood cells in human spleen and consequences for
895 hereditary blood disorders. *Proceedings of the National Academy of Sciences* **115**, 9574-9579
896 (2018).
897 77. R. K. Powers *et al.*, Trisomy 21 activates the kynurenine pathway via increased dosage of
898 interferon receptors. *Nat Commun* **10**, 4766 (2019).
899 78. H. Zheng *et al.*, C-Reactive protein and the kynurenic acid to quinolinic acid ratio are
900 independently associated with white matter integrity in major depressive disorder. *Brain Behav*
901 *Immun* **105**, 180-189 (2022).
902 79. T. Thomas *et al.*, Evidence of Structural Protein Damage and Membrane Lipid Remodeling in
903 Red Blood Cells from COVID-19 Patients. *Journal of Proteome Research* **19**, 4455-4469 (2020).
904 80. D. A. Bizjak *et al.*, SARS-CoV-2 Altered Hemorheological and Hematological Parameters
905 during One-Month Observation Period in Critically Ill COVID-19 Patients. *Int J Mol Sci* **23**,
906 (2022).
907 81. E. Nader *et al.*, Increased blood viscosity and red blood cell aggregation in patients with
908 COVID-19. *Am J Hematol* **97**, 283-292 (2022).
909 82. T. Nemkov, J. A. Reisz, S. Gehrke, K. C. Hansen, A. D'Alessandro, High-Throughput
910 Metabolomics: Isocratic and Gradient Mass Spectrometry-Based Methods. *Methods in*
911 *Molecular Biology (Clifton, N.J.)* **1978**, 13-26 (2019).
912 83. J. A. Reisz, C. Zheng, A. D'Alessandro, T. Nemkov, Untargeted and Semi-targeted Lipid
913 Analysis of Biological Samples Using Mass Spectrometry-Based Metabolomics. *Methods in*
914 *Molecular Biology (Clifton, N.J.)* **1978**, 121-135 (2019).
915 84. Z. Pang *et al.*, Using MetaboAnalyst 5.0 for LC-HRMS spectra processing, multi-omics
916 integration and covariate adjustment of global metabolomics data. *Nat Protoc* **17**, 1735-1761
917 (2022).

918 85. P. Shannon *et al.*, Cytoscape: a software environment for integrated models of biomolecular
919 interaction networks. *Genome Res* **13**, 2498-2504 (2003).
920 86. D. Stephenson, T. Nemkov, S. M. Qadri, W. P. Sheffield, A. D'Alessandro, Inductively-Coupled
921 Plasma Mass Spectrometry-Novel Insights From an Old Technology Into Stressed Red Blood
922 Cell Physiology. *Front Physiol* **13**, 828087 (2022).
923 87. R. Bruderer *et al.*, Extending the limits of quantitative proteome profiling with data-independent
924 acquisition and application to acetaminophen-treated three-dimensional liver microtissues. *Mol*
925 *Cell Proteomics* **14**, 1400-1410 (2015).
926 88. S. X. Ge, D. Jung, R. Yao, ShinyGO: a graphical gene-set enrichment tool for animals and
927 plants. *Bioinformatics* **36**, 2628-2629 (2019).
928 89. W. Luo, C. Brouwer, Pathview: an R/Bioconductor package for pathway-based data integration
929 and visualization. *Bioinformatics* **29**, 1830-1831 (2013).
930